ADAPTIVE SCENARIO GENERATION FOR KL-DRO AROUND A LEARNED DENSITY MODEL

Anonymous authors
Paper under double-blind review

ABSTRACT

Distributionally robust optimization (DRO) hedges data-driven two-stage stochastic programs against error in the distribution estimated from a finite record. Standard ambiguity sets treat realizations absent from the record in one of two ways. A divergence ball around the empirical distribution contains only reweightings of the record. A transport ball also contains distributions supported off the record, including on realizations the data-generating process cannot produce, against which the decision is then hedged. We propose a Kullback–Leibler (KL) ball centered at a density model fitted to the record, the learned nominal, so that the adversary can up-weight costly unobserved realizations in proportion to the probability the model assigns them. Because an independent sample of the few scenarios the problem can accommodate is likely to omit the rare realizations on which the worst case concentrates, we build the scenario set adaptively. We alternate between solving the finite problem and drawing new realizations from the learned nominal, steered toward the worst case at the current decision, with importance weights that keep the ball centered at the model. On a multi-item newsvendor problem and a capacity expansion problem on realistic grid data, centering the ball at the learned nominal rather than at the record lowers cost under distribution shift, at comparable in-distribution cost, when the record is scarce and the model class captures structure that lets it extrapolate beyond the record. The advantage fades as the record grows or as the shift departs from the structure the model has learned.

1 INTRODUCTION

Two-stage stochastic programs model decisions that must be committed before uncertainty is realized, with recourse actions taken after, in applications spanning finance, supply chains, telecommunications, and energy systems (Wallace & Ziemba, 2005; Birge & Louveaux, 2011). We consider their data-driven, *distributionally robust* form,

$$\min_{x\in\mathcal{X}} \Big\{ c(x) + \max_{\mathbb{P}\in\mathcal{P}(\mathbb{Q})} \mathcal{R}_{\mathbb{P}}\big[Q(x,\xi)\big] \Big\}, \qquad Q(x,\xi) \coloneqq \min_{y\in\mathcal{Y}(\xi,x)} q(y), \tag{1}$$

where x denotes here-and-now decisions with cost $c(x)$, $\xi \in \mathbb{R}^D$ the random vector, $Q(x,\xi)$ the cost of the wait-and-see decisions y, $\mathcal{P}(\mathbb{Q})$ an *ambiguity set* of distributions considered plausible around a nominal distribution $\mathbb{Q}$ (in the standard setting, the empirical distribution $\hat{\mathbb{Q}}_N$ of a record of N past realizations), and $\mathcal{R}_{\mathbb{P}}$ a risk measure, such as the expectation or the conditional value at risk (CVaR). We are motivated by problems whose cost is dominated by tail events, in which several dimensions of uncertainty move against the plan at once, such as a demand surge that arrives while a supplier is down.

Such problems expose two gaps in how data-driven distributionally robust optimization (DRO) treats realizations absent from the record. The first is in the ambiguity set (Sec. 3). Divergence balls around the empirical distribution contain only reweightings of the record, while Wasserstein balls and moment-based sets admit unobserved realizations judged by their distance from the record or by a few moments. Each family carries a finite-sample guarantee tied to the record (Duchi et al., 2021; Mohajerin Esfahani & Kuhn, 2018), but none uses how the components of the uncertainty move together in the tail, the structure that distinguishes plausible unobserved realizations from implausible ones. The second gap is in the finite scenario set on which the problem is solved, whose size is limited

Reviewers: please read the Reviewer Guidelines (iclr.cc/Conferences/2027/ReviewerGuidelines) and the AI Policy for Reviewers (iclr.cc/Conferences/2027/AIPolicyForReviewers). If you used AI to expand, edit, or polish your review, please provide the input text to the LLM. Better still, consider skipping the LLM and submitting your original text: we, and the authors, are much more interested in your unedited thoughts than in what an LLM has to say. AI-assisted or not, you are putting your name and reputation behind your review: LLM-generated falsehoods, hallucinations or misrepresentations are subject to disciplinary action, which may include desk-rejecting all papers you have authored.

because each scenario adds a copy of the recourse problem. A divergence ball can only reweight this set, and scenario reduction and problem-driven selection choose it from the record or from a sample drawn once, so the set is likely to miss the rare realizations on which the worst case concentrates.

High-resolution operational records, often spanning only a few years, are available in many applications of stochastic programming, and generative models trained on such records can capture their dependence structure and respect known properties of the process, including the behavior of its extremes (Boulaguiem et al., 2022; Pandey et al., 2025; Chang & Sapsis, 2026). Such models offer both a new center for the ambiguity set and a new source of scenarios, which raises the question of *how a generative model learned from a short record can be integrated into risk-averse stochastic programming, so that a limited set of scenarios hedges against tail risks the record underrepresents*.

We propose Kullback–Leibler DRO (KL-DRO) centered at a learned nominal: we take $\mathbb{Q}$ in equation 1 to be a density model $\mathbb{Q}_\theta$ trained on the record, such as a normalizing flow, a Gaussian copula, or a diffusion model, and the ambiguity set to be

$$\mathcal{P}_\rho(\mathbb{Q}_\theta) \coloneqq \big\{\mathbb{P} : \mathrm{KL}(\mathbb{P} \,\|\, \mathbb{Q}_\theta) \le \rho\big\}. \tag{2}$$

The adversary can then up-weight costly realizations absent from the record in proportion to the probability $\mathbb{Q}_\theta$ assigns them, and what it can reach is governed by the learned nominal rather than by a distance from the record. To close the second gap, we build the scenario set adaptively, alternating between solving the finite problem and drawing new realizations from the learned nominal, steered toward the worst case at the current decision, with importance weights that keep the ball centered at $\mathbb{Q}_\theta$. The learned nominal gives up the finite-sample guarantees of balls centered at the record, so the radius is chosen empirically (Sec. 5).

Contributions. Our contributions are as follows.

- **Distributionally robust optimization with a learned nominal.** We pose KL-DRO with the ambiguity set centered at a learned generative model, extending balls centered at parametric models or Bayesian posteriors for single-stage objectives (Watson & Holmes, 2016; Dellaporta et al., 2025) to high-dimensional nominals and two-stage objectives.
- **Finite scenario approximations for tail-dominated problems.** We build the scenario set by adaptive importance sampling toward the ball's worst case at each decision, so that the draws that reduce the variance of the estimated objective are those the adversary up-weights.
- **Evaluations in controlled and realistic settings.** We evaluate the framework on a multi-item newsvendor problem with a known law and controlled record size and shift, and on a capacity expansion problem over a 20-zone network with realistic demand and renewable data and an out-of-distribution test year.

2 Background

Risk-averse stochastic programming. Given a limited record of past realizations, we seek decisions that are cost-effective both *in distribution*, even when the record is too small to learn the data-generating process, and *out of distribution*, when that process changes at evaluation time. To weigh both typical and tail costs, we take $\mathcal{R}$ to be the mean–CVaR objective, which can be defined as the minimum over a scalar ζ of an expectation (Rockafellar & Uryasev, 2000),

$$\begin{aligned} \mathcal{R}_{\mathbb{P}}[Q(x,\xi)] &= (1-\beta)\,\mathbb{E}_{\mathbb{P}}[Q(x,\xi)] + \beta\,\mathrm{CVaR}_{\alpha,\mathbb{P}}[Q(x,\xi)] \\ &= \min_{\zeta\in\mathbb{R}} \big\{\zeta + \mathbb{E}_{\mathbb{P}}[\psi_\zeta(Q(x,\xi))]\big\}, \\ \psi_\zeta(u) &= (1-\beta)(u-\zeta) + \tfrac{\beta}{1-\alpha}\,(u-\zeta)_+, \end{aligned} \tag{3}$$

where α is the tail level, $\beta \in [0,1]$ the weight on the tail, and the minimizing ζ the value at risk at level α. Throughout, we assume that the recourse problem is feasible (relatively complete recourse) and bounded for every $x \in \mathcal{X}$ and every ξ in the support of the nominal, so that $Q(x,\xi)$ is finite.

Kullback–Leibler DRO. For a nominal distribution $\mathbb{Q}$, empirical or otherwise, the Kullback–Leibler (KL) ambiguity set $\{\mathbb{P} : \mathrm{KL}(\mathbb{P} \,\|\, \mathbb{Q}) \le \rho\}$ is a standard choice for two-stage problems

(Ben-Tal et al., 2013; Bayraksan & Love, 2015). Every member assigns zero probability wherever $\mathbb{Q}$ does, so the ball reweights the realizations $\mathbb{Q}$ supports and adds none. Centered at the empirical record, it changes only the probabilities of the recorded scenarios. Over this ball, the inner maximization of equation 1 can be reformulated as a minimization by dualizing the KL constraint (Hu & Hong, 2013; App. B.5),

$$\max_{\mathbb{P}\,:\,\mathrm{KL}(\mathbb{P}\,\|\,\mathbb{Q})\le\rho} \mathcal{R}_{\mathbb{P}}[Q(x,\xi)] = \min_{\zeta,\,\lambda>0} \Big\{ \zeta + \lambda\rho + \lambda \log \mathbb{E}_{\mathbb{Q}}\big[\exp\big(\psi_\zeta(Q(x,\xi))/\lambda\big)\big] \Big\}. \tag{4}$$

The dual is jointly convex in ζ and λ, and in x as well when the recourse cost is convex in x, as it is for linear recourse. For a finite nominal $\hat{\mathbb{Q}} = \sum_{i=1}^{K} w_i\, \delta_{\xi_i}$, a set of K scenarios with weights $w_i > 0$ summing to one, the expectation is a weighted sum, and equation 1 over the ball becomes, when $\mathcal{X}$ is convex, the single convex program

$$\min_{x\in\mathcal{X},\,\zeta,\,\lambda>0}\; c(x) + \zeta + \lambda\rho + \lambda \log \sum_{i=1}^{K} w_i \exp\big(\psi_\zeta(Q(x,\xi_i))/\lambda\big), \tag{5}$$

in which each scenario contributes one copy of the recourse problem and the risk measure adds one variable. The empirical measure $\hat{\mathbb{Q}}_N$ is the case $K = N$ and $w_i = 1/N$. The reformulation holds for any finite nominal, so two modeling choices remain: which realizations the adversary can reach, set by $\mathbb{Q}$, and which finite $\hat{\mathbb{Q}}$ the problem is solved on. We discuss these two aspects in turn.

Ambiguity centered at a learned nominal. The first aspect is which realizations the adversary can reach. Ideally, the nominal places mass on realizations the record lacks but not on those the data-generating process cannot produce, so that the decision is hedged against unrecorded events without paying for implausible ones. A density model $\mathbb{Q}_\theta$ fitted to the record places mass between and beyond the recorded realizations, distributed according to the dependence structure it has learned, so the ball around it contains distributions that weight events the record lacks. How well it withholds mass from implausible realizations depends on how faithfully it captures that structure. Because $\mathbb{Q}_\theta$ is itself an estimate, the ball around it also hedges against error in the model, as in Watson & Holmes (2016) and Dellaporta et al. (2025). We adopt the ambiguity set equation 2, the KL ball above centered at $\mathbb{Q}_\theta$ rather than at the record. We take $\mathbb{Q}_\theta$ to be the pushforward of the standard normal distribution $\varphi := \mathcal{N}(0, I)$, whose density we also write φ, by a deterministic decoder G_θ, so that sampling amounts to drawing $z \sim \varphi$ and applying G_θ. Normalizing flows, Gaussian copulas, and diffusion models with deterministic samplers are of this form, and the known latent density is what gives the sampler of Sec. 4 exact importance weights.

Finite scenario approximation. For the second aspect, the finite program equation 5, which we call the master problem, grows with each scenario, so the number of scenarios K must be small, and the decision is largely determined by which K scenarios the master sees. When the realizations that drive the decision are rare, such as the few shock days on which a portfolio incurs most of its losses, K independent draws are likely to miss them. Scenario reduction and problem-driven selection choose the K scenarios from a larger pool (Sec. 3), but a pool fixed in advance cannot supply realizations it lacks. A learned nominal can instead be sampled wherever it has mass, so the K scenarios can be generated where the decision is sensitive. Because they are not drawn from $\mathbb{Q}_\theta$ itself, each carries a base weight w_i, an importance weight back to $\mathbb{Q}_\theta$, and we solve equation 5 with these weights normalized to sum to one, which keeps the ball centered at $\mathbb{Q}_\theta$ rather than at the distribution the scenarios were drawn from.

3 Related Work

Ambiguity sets. Divergence-based sets (Ben-Tal et al., 2013; Bayraksan & Love, 2015) reweight the empirical record and so preclude unobserved realizations, or, with the arguments of the divergence reversed, admit them only on a fixed finite support (Van Parys et al., 2021). Transport-based sets (Mohajerin Esfahani & Kuhn, 2018; Gao & Kleywegt, 2023) admit them, but judge them by a cost that measures how far a recorded point moves and says nothing directly about whether the moved point is plausible. The Sinkhorn variant smooths this cost against a reference measure chosen in advance, such as a Gaussian, which sets where the worst case can place mass (Wang et al., 2021).

Moment-based sets (Delage & Ye, 2010) constrain only low-order statistics. Closest in motivation are works that learn part of the set: the transport cost, from labels or the data manifold (Blanchet et al., 2019; Liu et al., 2022), or the nominal itself, a fitted model or Bayesian posterior at which a KL-based set is centered (Watson & Holmes, 2016; Dellaporta et al., 2025).

Scenario construction. Distribution-driven methods match specified moments (Høyland et al., 2003) or reduce a pool under a probability metric (Dupačová et al., 2003; Heitsch & Römisch, 2003) without reference to the decision. Problem-driven methods cluster by decision-based dissimilarity or minimize implementation error (Hewitt et al., 2022; Keutchayan et al., 2023), or, for tail risk measures, sample only the region of the support on which the risk measure depends (Fairbrother et al., 2022). All of these methods construct the set once, before the problem is solved, whereas the importance sampling methods of Sec. 4 adapt the proposal to the decision.

Generative models in optimization. A more recent line of work samples scenarios from a generative model fitted to the record (Chen et al., 2018; Jiang et al., 2018) or trains the generator on the downstream decision loss (Zhao et al., 2026; Islip et al., 2025), producing scenarios but no ambiguity set. A second line makes the generator the adversary, through a learned transport map to a continuous least favorable distribution (Xu et al., 2024; Cheng et al., 2025), a family of parametric generative models within a KL budget (Michel et al., 2021), a family of generators of bounded reconstruction loss (Wen & Yang, 2026), a Sinkhorn comparison between conditional generators (Zhang et al., 2026), or, for two-stage robust optimization, a search of a generator's latent space for a single worst-case realization (Brenner et al., 2025). In each, the worst case is obtained by optimizing over that parameterization, and all but the last are posed for single-stage objectives. We instead center a divergence ball at the generator, which leaves the generator as trained, gives the worst case in closed form, and keeps the likelihood ratios exact.

4 Adaptive Importance Sampling Algorithm

Section 2 called for a finite scenario set generated where the decision is sensitive and weighted back to $\mathbb{Q}_\theta$. We propose building it iteratively by adaptive importance sampling toward a target known up to a normalizing constant (Bugallo et al., 2017), re-targeting as the decision changes, as Dantzig & Glynn (1990), Infanger (1992), Parpas et al. (2015), and Aolaritei et al. (2026) do for a known density. Each round tilts a sample of the model toward the worst case at the current decision and forms the batch either by resampling that sample, which needs only draws of the model, or by drawing from a Gaussian fitted to the tilt by weighted moment matching, a cross-entropy step (Rubinstein & Kroese, 2004) that can reach realizations beyond the initial sample. What distinguishes our approach is the target and the nominal. First, our target is the worst case of the KL ball, so the draws reduce the variance of the estimated objective and supply the realizations the adversary up-weights (Sec. 4.2), whereas Aolaritei et al. (2026) target the variance of a stochastic gradient. Second, we draw from a learned density model (Sec. 4.3), whereas the methods above assume a known density and Parpas et al. (2015) fit a kernel density estimate to Markov chain samples, which degrades in high dimension. Kim et al. (2025) steer a generative model toward costly inputs with importance weights, but to train a predictor. Figure 1 summarizes the framework.

4.1 Alternating Master and Sampler

The master on the scenario set. Each round draws a batch of n scenarios at the incumbent x_t with base weights back to the nominal (Sec. 4.3), adds it to the set held, and solves equation 5 on that set for x_{t+1} (Algorithm 1). A batch's weights depend on its proposal alone and have expectation one, so a batch drawn at x_t estimates the nominal expected cost without bias at every x. Because equation 5 requires weights that sum to one, the weights of all rounds are normalized together, $\bar{w}_i = w_i / \sum_j w_j$ over the K_{t+1} scenarios held. Dividing by their random total biases the estimate for finite K_{t+1}, but the bias vanishes as K_{t+1} grows, so the estimate is consistent. The master on the held scenarios is

$$\min_{x \in \mathcal{X},\, \zeta,\, \lambda > 0} \; c(x) + \zeta + \lambda\rho + \lambda \log \sum_{i=1}^{K_{t+1}} \bar{w}_i \exp\big(\psi_\zeta(Q(x, \xi_i))/\lambda\big). \tag{6}$$

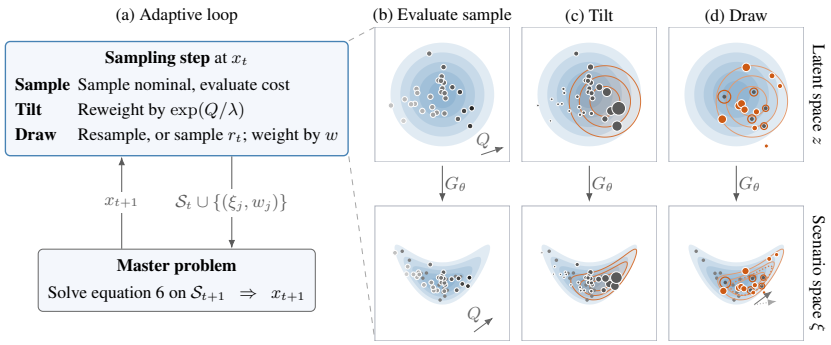


Figure 1: **(a)** The adaptive loop. **(b–d)** One sampling step in a 2-D slice of the latent space (contours of φ; cost rises to the upper right): (b) an initial sample is evaluated; (c) it is tilted by $\exp(Q/\lambda)$, and a Gaussian proposal g_t (orange) is fitted; (d) new scenarios are resampled (rings) or drawn from the proposal (filled), with weights back to the nominal (marker area). **Bottom row.** The same steps after decoding by G_θ: new scenarios reach beyond the record (gray), and the target moves with the decision (dotted).

Its worst case at a decision x is $p_i \propto \bar{w}_i \exp(\psi_{\zeta^*}(Q(x, \xi_i))/\lambda^*)$, where ζ^* and λ^* attain the minimum at x, so that $\mathrm{KL}(p \,\|\, \bar{w}) = \rho$. When equation 6 is too large to solve jointly, it can instead be solved with the weights fixed at the worst case computed at x_t, which requires K_t recourse evaluations. Weak duality then bounds the resulting optimality gap on the held scenarios at the cost of one more master solve (App. B.5).

Sampler and radii. The sampler targets the worst case under the expectation, which, because ψ_ζ is nondecreasing, ranks scenarios by cost as the mean–CVaR worst case does. Since the weights correct any proposal back to the nominal, this choice affects efficiency but not the consistency of the estimated objective. It tilts an initial sample of M draws from the nominal at a reference radius ρ_{ref}, $\tau_i \propto \exp(Q(x_t, \xi_i)/\lambda_t)$ with $\sum_i \tau_i \log(M\tau_i) = \rho_{\mathrm{ref}}$. Thus ρ_{ref} determines which scenarios enter the set and ρ how the master weights them, and $\rho = 0$ with $\rho_{\mathrm{ref}} > 0$ solves the nominal problem with a decision-aware sampler. We take $\rho_{\mathrm{ref}} \geq \rho$ as a heuristic, because a sampler that reaches beyond the adversary only costs efficiency, whereas one that reaches less leaves tail scenarios out of the set, and no reweighting can restore them. Each initial sample costs M recourse evaluations, which run in parallel, whereas only the batch of n enters the master, whose size grows with each scenario. The tilt depends on the decision only through the costs at x_t, so it changes little once the incumbent settles, and the initial sample need only be redrawn and re-tilted in the rounds $t \in \mathcal{T}$. Later batches reuse the last initial sample and proposal, and their weights remain exact.

Algorithm 1 Adaptive scenario acquisition.

Require: Nominal $\mathbb{Q}$ that can be sampled; radii ρ and ρ_{ref}; initial sample size M; batch size n; rounds T; re-targeting rounds $\mathcal{T} \ni 0$; mixture weight a

Choose an initial decision x_0; set $\mathcal{S}_0 \leftarrow \emptyset$
for $t = 0, \ldots, T-1$ **do**
  if $t \in \mathcal{T}$ **then** ▷ Re-target; otherwise keep the last
    Draw $\xi_1, \ldots, \xi_M \sim \mathbb{Q}$ and evaluate $Q_i \leftarrow Q(x_t, \xi_i)$ ▷ Initial sample
    Bisect λ_t so that $\tau_i \propto \exp(Q_i/\lambda_t)$ satisfies $\sum_i \tau_i \log(M\tau_i) = \rho_{\mathrm{ref}}$ ▷ Tilt
  end if
  if resampling **then**
    Resample n indices $\propto \tau$; $\mathcal{B}_t \leftarrow \{(\xi_i, c_i/(M\tau_i))\}$ over distinct i ▷ Resampling
  else
    Fit g_t to the tilted latent points of the initial sample ▷ Fitted proposal
    Draw from $r_t = (1-a)\,\varphi + a\, g_t$ with weights φ/r_t; keep n draws as $\mathcal{B}_t$, or resample n by the tilt as above
  end if
  $\mathcal{S}_{t+1} \leftarrow \mathcal{S}_t \cup \mathcal{B}_t$
  Solve equation 6 on $\mathcal{S}_{t+1}$ for x_{t+1} ▷ Master
end for
return x_T

4.2 The Sampling Target

Latent space. The sampler works in the latent space, where the nominal is the standard Gaussian φ. Because φ is known, a proposal from a simple parametric family has likelihood ratios in closed form there, without evaluating the density of $\mathbb{Q}_\theta$, and these ratios correct the expectation of any function of z, including the cost $Q(x, G_\theta(z))$ of the decoded scenario. In the ambient space, such a family would match $\mathbb{Q}_\theta$ poorly. The problem can be posed in the latent space entirely,

$$\min_{x \in \mathcal{X}} \Big\{ c(x) + \max_{p \,:\, \mathrm{KL}(p \,\|\, \varphi) \le \rho} \mathcal{R}_{z \sim p}\big[Q(x, G_\theta(z))\big] \Big\}, \tag{7}$$

in which the adversary reweights φ. Decoding maps this latent ball onto the ball around $\mathbb{Q}_\theta$ for any measurable G_θ. Pushing two distributions through the same map cannot increase the divergence between them (the data-processing inequality; Cover & Thomas, 2006), so the latent ball decodes into the ambient ball. Conversely, any $\mathbb{P}$ in the ambient ball is the image of φ reweighted by $\frac{d\mathbb{P}}{d\mathbb{Q}_\theta} \circ G_\theta$, whose divergence from φ equals $\mathrm{KL}(\mathbb{P} \,\|\, \mathbb{Q}_\theta)$. For a law-invariant $\mathcal{R}$, such as the expectation and CVaR (Kuhn et al., 2025, Def. 5.1), the two problems therefore have the same value and minimizers, whether or not G_θ is invertible.

The tilt as a proposal. Under the expectation, the worst case of equation 7 at a fixed decision is the exponential tilt

$$\pi(z \mid x) \;\propto\; \varphi(z)\, \exp\big(Q(x, G_\theta(z))/\lambda\big), \tag{8}$$

with λ fixed by the radius. The tilt weights a realization by the level of its cost, whereas the decision responds only to the part of the cost that x can change. The level is a faithful proxy when the costly realizations are those the decision can mitigate, such as unserved load that added capacity would avert, and fails when the costliest realizations are costly whatever the decision, since the tilt then concentrates the sample where the master cannot respond. Read as robustness, $\pi(\cdot \mid x)$ is the least favorable distribution; read as estimation, it is the exponential tilting of rare-event sampling (Blanchet & Lam, 2011). For large λ it is close to a mixture of φ and the minimum-variance proposal, which reweights φ by the cost itself when the cost is nonnegative. For small λ, it concentrates on the costliest scenarios, where the master's worst case places its weight. For any proposal g positive wherever φ is, draws $z_j \sim g$ with the weight

$$w(z) = \varphi(z)/g(z) \tag{9}$$

give an unbiased estimate $\frac{1}{n} \sum_j w(z_j)\, Q(x, G_\theta(z_j))$ of $\mathbb{E}_\varphi[Q(x, G_\theta(z))]$.

4.3 Drawing the Batch

The target equation 8 is known only through evaluations of Q, each a second-stage solve. Guided sampling of the generator yields draws without likelihood ratios, and Markov chain Monte Carlo (Parpas et al., 2015) needs many sequential evaluations of Q per retained sample. We instead form the batch from the tilt τ of the initial sample in one of two ways.

Resampling. Resample n indices with probabilities τ. A scenario drawn c_i times enters with base weight $w_i = c_i/(M\tau_i)$, which corrects the selection back to the nominal. The batch holds only realizations in the initial sample, so its reach is governed by M. Because it needs only draws, resampling also applies to models available only as samplers and to the empirical measure.

Fitted proposal. Fit a Gaussian $g_t = \mathcal{N}(\hat{\mu}, \hat{\Sigma})$ to the latent points z_i of the initial sample, $\xi_i = G_\theta(z_i)$, weighted by the tilt: $\hat{\mu} = \sum_i \tau_i z_i$ and $\hat{\Sigma} = \sum_i \tau_i (z_i - \hat{\mu})(z_i - \hat{\mu})^\top$. When the M evaluations are few relative to the latent dimension, $\hat{\Sigma}$ can be regularized, for example by shrinkage toward its diagonal or, at the extreme, by fixing $\hat{\Sigma} = I$ so that only the mean shifts. Draw from the defensive mixture $r_t = (1 - a)\, \varphi + a\, g_t$ with $a \in (0, 1)$, decode $\xi = G_\theta(z)$, and attach the weight

$$w(z) = \frac{\varphi(z)}{r_t(z)} = \Big[(1 - a) + a\, \frac{g_t(z)}{\varphi(z)}\Big]^{-1} \le \frac{1}{1 - a}, \tag{10}$$

with g_t/φ in closed form. The weight is exact however g_t was fitted, and the component φ bounds it, so a poor fit lowers efficiency but cannot produce an unbounded weight. The draws either enter the master directly with the weights equation 10 or form a pool from which n are resampled by the tilt as above, with the uniform weights $1/M$ replaced by the normalized weights of equation 10 (App. B.4).

Choosing a variant. Resampling needs only draws of the nominal, but its weights vary with the tilt, so a concentrated tilt and a small n give a noisy correction. The fitted proposal reaches beyond the initial sample with every weight below $1/(1-a)$, but it needs latent coordinates and a proposal family that fits the tilt, a fit that degrades with dimension. It should therefore help most when the events that drive the worst case are rare in an initial sample of size M and the tilted target is close to a single Gaussian in the latent space, and least when decoded draws cannot leave the record's range or the map from z to a scenario is strongly nonlinear (Sec. 5.1).

5 EXPERIMENTS

We evaluate the framework in two settings. In a multi-item newsvendor problem, a standard testbed for DRO (Scarf, 1958; Hanasusanto et al., 2015; Ban & Rudin, 2019), the demand law is known, so optimality gaps can be computed accurately, and the record size and the shift are under our control, so we can isolate the regimes in which a learned nominal improves on the record. A capacity expansion problem for the Texas grid on realistic data tests whether the framework carries over to a planning problem of practical scale.

Methods. All methods solve the master equation 5 on a finite scenario set and differ in where the scenarios come from, how they are chosen, and how the master hedges. Our method draws scenarios from a learned nominal, either by resampling its draws (KL-Gen) or from a proposal fitted to the tilt (KL-Gen-P), chooses them by the tilt at the current decision, and hedges with a KL ball. The comparators are grouped by the component they change. *Source:* KL-DRO centered at the record (KL-Rec) removes generation; KL-DRO over record points moved toward higher cost by optimal transport (KL-OT) extrapolates by distance from the record instead of by a model; alternative nominals isolate the model class; and in the newsvendor an oracle applies our sampler to the true law. *Selection:* cost-space scenario clustering (CSSC; Keutchayan et al., 2023) chooses scenarios once, by their effect on the decision. *Hedge:* sample average approximation (SAA) applies none, and Wasserstein DRO (W-DRO; Mohajerin Esfahani & Kuhn, 2018) hedges with a transport ball around the record. Both studies use the mean–CVaR objective with $\beta = 0.25$ and $\alpha = 0.9$. Tables 2 and 9 give the implementations. Because hedging can lower out-of-distribution cost at the expense of in-distribution cost, we compare the frontiers of out-of-distribution (OOD) against in-distribution (ID) cost that each method's settings trace.

5.1 MULTI-ITEM NEWSVENDOR WITH SUBSTITUTION

Problem. A retailer orders five products at a cost of 1 per unit before demand is observed. As recourse, unmet demand for a product can be served from the next product's stock at a penalty of 0.5 per unit (substitution) or lost at a cost of 100 per unit, and leftover stock is salvaged at 0.25. For a single product, the order that minimizes expected cost is the quantile of demand at the critical ratio $(100-1)/(100-0.25) \approx 0.99$, and the mean–CVaR objective used here raises it further, so the orders lie in the upper tail of demand. Log demand follows a known Gaussian mixture with a rare shock that raises demand for every product at once (App. A). A decision-maker sees a record of $N \in \{16, 32, 64, 128\}$ periods and is scored under one of four shifted laws: a level shift in every product's demand, a tail shift to a heavier-tailed shock, a support shift that adds a shock on different products, and a coincidence shift, in which the record's shocks strike one product at a time and the test law's strike all products together, with unchanged marginals.

Setup. For each record we fit five learned nominals: a Gaussian copula; a log-normal; a two-component log-normal mixture, the family of the base law; a RealNVP flow; and a Gaussian fitted to raw demand, which captures dependence only through its covariance. KL-Gen-P, KL-Gen, and the oracle run a single round ($T = 1$) from the risk-neutral decision on the record. Costs are percentages above the optimum under the law in question. Table 1 reads the frontiers in two ways: (a) the OOD cost within an ID budget of 5 points over SAA, chosen on held-out records without the shifted law, and (b) the ID cost needed to halve SAA's OOD cost, which prices protection but is not a deployable rule.

Short records and coincident shocks favor generation. The optimal order depends on each product's top 1% of demand, which lies above the record's maximum in 85% of records at $N = 16$. Reweighting the record cannot reach it, so KL-Rec costs as much as SAA at every N. At $N = 16$,

Table 1: Newsvendor: cost above the optimum (%, median over records) under the level (L), tail (T), support (S), and coincidence (C) shifts. **(a)** Out-of-distribution cost at each method's selection rule. **(b)** In-distribution cost needed to halve SAA's out-of-distribution cost; ·: never reached; †: lowest in under 80% of bootstrap resamples. Bold: lowest among the rows shown.

	(a) OOD cost at SAA's ID budget								(b) ID cost to halve SAA's OOD cost							
	$N = 16$				$N = 128$				$N = 16$				$N = 128$			
Method	L	T	S	C	L	T	S	C	L	T	S	C	L	T	S	C
SAA	643	154	434	244	129	88	98	39	·	·	·	·	·	·	·	·
KL-Rec	647	155	435	227	141	89	111	39	·	·	·	·	·	·	·	·
W-DRO	80	**39**	92	154	**24**	**45**	**30**	18	55	68	55	97	12	42	12	20
KL-OT	88	43	99	159	45	57	44	25	57	64	57	97	12	**29**	12	·
KL-Gen-P																
Log-normal	52	52	47	**31**	35	56	35	**15**	21	23	21	24	**9**†	·	**9**†	**15**
Flow	**52**	52	**43**	33	41	58	35	18	**19**	**19**	**19**	**23**†	11	·	9	19
Gaussian	229	104	158	49	250	107	174	51	40	·	40	42	·	·	·	·
KL-Gen (flow)	229	103	152	49	206	101	138	46	36	·	36	33	·	·	·	·

KL-Gen-P with the log-normal or the flow halves SAA's OOD cost at about a third of the ID cost that W-DRO and KL-OT need (Table 1b). Which method leads then depends on the shift (Table 1a). W-DRO leads under the tail shift at every N and overtakes KL-Gen-P under the level and support shifts as N grows. KL-Gen-P stays lowest under the coincidence shift, because a fitted nominal places mass on joint shocks, which transport reaches only by moving every product of a record point at once.

The proposal helps when the nominal has the right tail. At the same 356 cost evaluations, KL-Gen-P cuts the out-of-distribution cost of KL-Gen by a factor of two to six under the level and support shifts for every nominal fitted to log demand other than the copula (Tables 3–6), since only about four of 356 draws from a nominal exceed a product's 99th percentile, whereas the proposal draws there directly (Sec. 4.3). CSSC, which reduces a pool of 1,024 generated draws at 95 times the evaluations, costs as much as KL-Gen: a larger generated pool does not substitute for sampling toward the worst case. For the copula, whose draws stay within the record's range, the proposal gains at most a factor of two. The nominal's tail matters more than its exact family: with the proposal, the log-normal costs less out of distribution than the Gaussian in every cell, and less than the log-normal mixture, the correctly specified family, under the level and support shifts up to $N = 64$ and under the coincidence shift at every N. These results support training generative models to reproduce the extremes of the process accurately (Jaini et al., 2020; Laszkiewicz et al., 2022; Pandey et al., 2025).

5.2 Capacity Expansion Planning

Problem. A planner sizes wind, solar, gas, and battery capacity in 20 zones of the Texas system, and transmission between them, within a capital budget, then dispatches hourly over a day of uncertain zonal demand and renewable availability ($D = 1{,}440$). Unserved load costs \$10,000/MWh, so cost is dominated by the few days on which high demand coincides with low renewable output across zones, and a record of a year or less rarely holds the worst of them.

Setup. A record of k years is every second day of one year of 2001–2010 ($k = \frac{1}{2}$) or a full year ($k = 1$), and App. B.7 adds five-year records ($k = 5$). The learned nominal is a seasonally conditioned normalizing flow fitted to the record alone and decoded through the record's marginal distributions (App. B.3). The objective is annualized capital cost plus the mean–CVaR of operating cost, with the same capital budget for every method. Every method holds at most $K = 48$ scenarios, the adaptive methods re-target every round, and the tables report KL-OT and W-DRO at the transport budget $\delta = 1$ (App. B.4). Decisions are scored by the objective, in bn\$/yr, on every day of 2011–2014 (ID), the four years after the record decade, and of 2020 (OOD), the most extreme year of 2001–2020 in the tail of demand (App. B.2).

Adaptive sampling helps throughout, and generation adds value on short records. Adaptive sampling alone cuts cost well below a static set of record days: at $\rho = 0$, KL-Rec is far cheaper than SAA at every k (Table 10). At $k = \frac{1}{2}$, every setting of KL-Rec and KL-OT is dominated in median cost by a setting of KL-Gen (Figure 2(a)). Over the three k, KL-Gen is cheaper than KL-OT out of distribu-

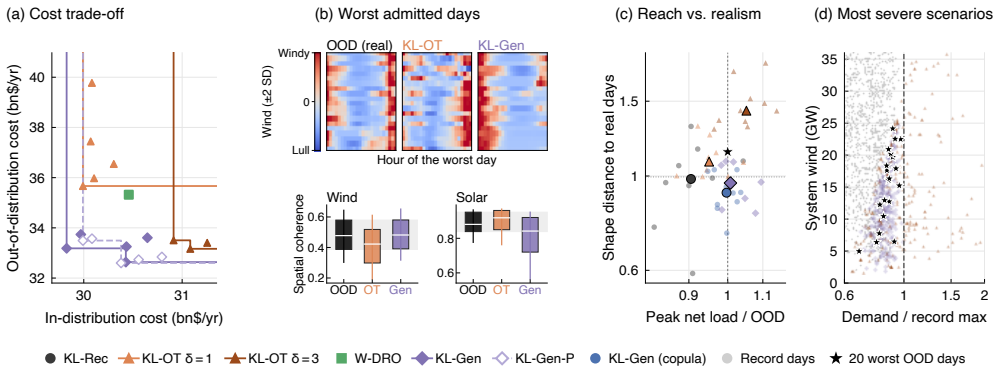


Figure 2: Capacity expansion at $k = \frac{1}{2}$ (panels defined in App. B.6). **(a)** OOD against ID cost (bn$/yr) of each setting, with Pareto frontiers; KL-Rec, CSSC, and SAA lie outside the range. **(b)** Zonal wind on the most severe OOD day and admitted scenarios (top), and their spatial coherence (bottom). **(c)** Severity against demand-rescaled distance to the nearest real day, for the most severe admitted scenarios. **(d)** Demand relative to its 2001–2010 maximum against system wind; stars: the 20 most severe OOD days.

tion at 14 of the 15 radius pairs, at a small in-distribution premium for $k \geq 1$ (Table 11). The advantage narrows as the record grows: KL-OT joins the front at $k = 1$ and KL-Rec at $k = 5$, whereas SAA, CSSC, and W-DRO never reach it. KL-Gen-P and KL-Gen with a seasonal Gaussian copula stay close to KL-Gen. The copula appears to capture what these decisions need, although the flow fits held-out days better (App. B.3), and at this dimension the fitted proposal adds little over resampling (Sec. 4.3).

The generator extrapolates structure the record already shows. The most severe days of 2020 lie within the demand range of 2001–2010 and are severe because high demand coincides with low renewable output across zones (panel d), a pattern present even in a $k = \frac{1}{2}$ record. The flow reproduces it: its most severe scenarios reach the OOD days' severity with spatial shapes as close to real days as the record's own severe days (panel c) and wind as spatially coherent as on real days (panel b).

Transport extrapolates in a direction real days do not take. KL-OT makes scenarios costly by inflating demand zone by zone, up to nearly twice the highest system demand of 2001–2010 at $\delta = 3$ (panel d), whereas on real days each zone's demand moves with the system total. At $\delta = 1$ its most severe scenarios fall just short of the OOD days' severity, and at $\delta = 3$ they reach it only with shapes farther from real days than the record's own severe days (panel c). Widening the transport budget brings its OOD cost toward that of KL-Gen only at a higher ID cost (panel a), a premium paid every year against days unlike those in the data, whereas KL-Gen's reach follows the structure it has learned.

6 Conclusion

For two-stage stochastic programs with severe tail risk, we proposed centering a KL ball at a generative model of a short record, so that the adversary judges unobserved realizations by learned dependence rather than distance from the record, and solving the resulting problem on scenarios drawn adaptively toward its worst case. In experiments, we found that the learned nominal helps most when the record is short and the model class extrapolates along structure the record shows, such as the co-movement of shocks or renewable shortfalls across products or zones. The advantage fades as the record grows, and transport around the record hedges more cheaply against shifts the model class does not anticipate. A fitted proposal adds most when the realizations driving the worst case are rare among the model's draws.

Limitations. Our work has both experimental and theoretical limitations. Experimentally, both case studies have linear recourse, so integer and nonlinear convex recourse remain untested. Theoretically, the ball around $\mathbb{Q}_\theta$ contains a law $\mathbb{P}$, shifted or not, only if $\rho \geq \mathrm{KL}(\mathbb{P} \,\|\, \mathbb{Q}_\theta)$. This divergence is set by the model's misspecification, which the record does not reveal, and is infinite if the model assigns no mass where $\mathbb{P}$ has some, as nominals decoded through the record's empirical marginals do beyond its range. We therefore choose the radius empirically, without a finite-sample guarantee.

AI USE STATEMENT

The authors received assistance from Claude Code in implementing the methods and baselines, producing the tables and figures from the data of the computational experiments, reviewing the literature, and editing and revising the text, and take full responsibility for the content of the paper.

REFERENCES

Liviu Aolaritei, Bart P. G. Van Parys, Henry Lam, and Michael I. Jordan. Stochastic Optimization with Optimal Importance Sampling, February 2026. URL http://arxiv.org/abs/2504.03560. arXiv:2504.03560 [math].

Gah-Yi Ban and Cynthia Rudin. The Big Data Newsvendor: Practical Insights from Machine Learning. *Operations Research*, 67(1):90–108, 2019. doi: 10.1287/opre.2018.1757.

Güzin Bayraksan and David K. Love. Data-Driven Stochastic Programming Using Phi-Divergences. In Dionne Aleman, Aurélie Thiele, J. Cole Smith, and Harvey J. Greenberg (eds.), *The Operations Research Revolution*, pp. 1–19. INFORMS, September 2015. ISBN 978-0-9843378-8-0. doi: 10.1287/educ.2015.0134. URL http://pubsonline.informs.org/doi/10.1287/educ.2015.0134.

Aharon Ben-Tal, Dick Den Hertog, Anja De Waegenaere, Bertrand Melenberg, and Gijs Rennen. Robust Solutions of Optimization Problems Affected by Uncertain Probabilities. *Management Science*, 59(2):341–357, February 2013. ISSN 0025-1909, 1526-5501. doi: 10.1287/mnsc.1120.1641. URL https://pubsonline.informs.org/doi/10.1287/mnsc.1120.1641.

John R. Birge and François Louveaux. *Introduction to Stochastic Programming*. Springer, 2 edition, 2011.

Jose Blanchet and Henry Lam. Rare event simulation techniques. In S. Jain, R. R. Creasey, J. Himmelspach, K. P. White, and M. Fu (eds.), *Proceedings of the 2011 Winter Simulation Conference*, pp. 146–160, 2011.

Jose Blanchet, Yang Kang, Karthyek Murthy, and Fan Zhang. Data-driven optimal transport cost selection for distributionally robust optimization. In *Proceedings of the Winter Simulation Conference*, 2019.

Younes Boulaguiem, Jakob Zscheischler, Edoardo Vignotto, Karin van der Wiel, and Sebastian Engelke. Modeling and simulating spatial extremes by combining extreme value theory with generative adversarial networks. *Environmental Data Science*, 1:e5, 2022. doi: 10.1017/eds.2022.4.

Cameron Bracken, Travis Thurber, and Nathalie Voisin. Hourly wind and solar generation profiles at 1/8th degree resolution, 2023. URL https://zenodo.org/records/10214348. Dataset.

Aron Brenner, Rahman Khorramfar, Jennifer Z. Sun, and Saurabh Amin. A deep generative learning approach for two-stage adaptive robust optimization. In *International Conference on Learning Representations*, 2025.

Mónica F. Bugallo, Víctor Elvira, Luca Martino, David Luengo, Joaquín Míguez, and Petar M. Djurić. Adaptive importance sampling: The past, the present, and the future. *IEEE Signal Processing Magazine*, 34(4):60–79, 2017. doi: 10.1109/MSP.2017.2699226.

Kai Chang and Themistoklis P. Sapsis. Extreme event aware (η-) learning. *Nature Communications*, 2026. doi: 10.1038/s41467-026-76811-x. arXiv:2510.19161.

Yize Chen, Yishen Wang, Daniel Kirschen, and Baosen Zhang. Model-free renewable scenario generation using generative adversarial networks. *IEEE Transactions on Power Systems*, 33(3):3265–3275, 2018.

Xiuyuan Cheng, Yao Xie, Linglingzhi Zhu, and Yunqin Zhu. Worst-case generation via minimax optimization in Wasserstein space, December 2025. URL http://arxiv.org/abs/2512.08176. arXiv:2512.08176 [stat].

Paul G. Constantine. *Active Subspaces: Emerging Ideas for Dimension Reduction in Parameter Studies*. Society for Industrial and Applied Mathematics, 2015. doi: 10.1137/1.9781611973860.

Thomas M. Cover and Joy A. Thomas. *Elements of Information Theory*. Wiley, 2nd edition, 2006.

George B. Dantzig and Peter W. Glynn. Parallel processors for planning under uncertainty. *Annals of Operations Research*, 22:1–21, 1990. doi: 10.1007/BF02023045.

Erick Delage and Yinyu Ye. Distributionally Robust Optimization Under Moment Uncertainty with Application to Data-Driven Problems. *Operations Research*, 58(3):595–612, 2010. doi: 10.1287/opre.1090.0741.

Charita Dellaporta, Patrick O'Hara, and Theodoros Damoulas. Decision making under the exponential family: Distributionally robust optimisation with bayesian ambiguity sets. In *Proceedings of the 42nd International Conference on Machine Learning*, 2025.

Steven Diamond and Stephen Boyd. CVXPY: A Python-embedded modeling language for convex optimization. *Journal of Machine Learning Research*, 17(83):1–5, 2016.

Laurent Dinh, Jascha Sohl-Dickstein, and Samy Bengio. Density estimation using Real NVP. February 2017. URL https://openreview.net/forum?id=HkpbnH9lx.

John C. Duchi, Peter W. Glynn, and Hongseok Namkoong. Statistics of robust optimization: A generalized empirical likelihood approach. *Mathematics of Operations Research*, 46(3):946–969, 2021. doi: 10.1287/moor.2020.1085.

J. Dupačová, N. Gröwe-Kuska, and W. Römisch. Scenario reduction in stochastic programming. *Mathematical Programming*, 95(3):493–511, March 2003. ISSN 0025-5610, 1436-4646. doi: 10.1007/s10107-002-0331-0. URL http://link.springer.com/10.1007/s10107-002-0331-0.

Jamie Fairbrother, Amanda Turner, and Stein W. Wallace. Problem-driven scenario generation: an analytical approach for stochastic programs with tail risk measure. *Mathematical Programming*, 191(1):141–182, January 2022. ISSN 0025-5610, 1436-4646. doi: 10.1007/s10107-019-01451-7. URL https://link.springer.com/10.1007/s10107-019-01451-7.

Rui Gao and Anton Kleywegt. Distributionally Robust Stochastic Optimization with Wasserstein Distance. *Mathematics of Operations Research*, 48(2):603–655, 2023. doi: 10.1287/moor.2022.1275.

Paul J. Goulart and Yuwen Chen. Clarabel: An interior-point solver for conic programs with quadratic objectives, 2024.

Gurobi Optimization, LLC. Gurobi Optimizer Reference Manual, 2026. URL https://www.gurobi.com.

Grani A. Hanasusanto, Daniel Kuhn, Stein W. Wallace, and Steve Zymler. Distributionally robust multi-item newsvendor problems with multimodal demand distributions. *Mathematical Programming*, 152(1-2):1–32, 2015. doi: 10.1007/s10107-014-0776-y.

Holger Heitsch and Werner Römisch. Scenario Reduction Algorithms in Stochastic Programming. *Computational Optimization and Applications*, 24(2):187–206, February 2003. ISSN 1573-2894. doi: 10.1023/A:1021805924152. URL https://doi.org/10.1023/A:1021805924152.

Mike Hewitt, Janosch Ortmann, and Walter Rei. Decision-based scenario clustering for decision-making under uncertainty. *Annals of Operations Research*, 315(2):747–771, August 2022. ISSN 0254-5330, 1572-9338. doi: 10.1007/s10479-020-03843-x. URL https://link.springer.com/10.1007/s10479-020-03843-x.

Zhaolin Hu and L. Jeff Hong. Kullback-Leibler divergence constrained distributionally robust optimization. Optimization Online, 2013.

Kjetil Høyland, Michal Kaut, and Stein W Wallace. A Heuristic for Moment-matching Scenario Generation. *Computational Optimization and Applications*, 24(2–3):169–185, 2003.

Gerd Infanger. Monte Carlo (importance) sampling within a benders decomposition algorithm for stochastic linear programs. *Annals of Operations Research*, 39(1):69–95, December 1992. ISSN 0254-5330, 1572-9338. doi: 10.1007/BF02060936. URL http://link.springer.com/10.1007/BF02060936.

David Islip, Roy H. Kwon, Sanghyeon Bae, and Woo Chang Kim. Contextual scenario generation for two-stage stochastic programming, 2025. URL https://arxiv.org/abs/2502.05349.

Priyank Jaini, Ivan Kobyzev, Yaoliang Yu, and Marcus Brubaker. Tails of Lipschitz triangular flows. In *Proceedings of the 37th International Conference on Machine Learning*, 2020.

Congmei Jiang, Yongfang Mao, Yi Chai, Mingbiao Yu, and Songbing Tao. Scenario generation for wind power using improved generative adversarial networks. *IEEE Access*, 6:62193–62203, 2018. doi: 10.1109/ACCESS.2018.2875936.

Julien Keutchayan, Janosch Ortmann, and Walter Rei. Problem-driven scenario clustering in stochastic optimization. *Computational Management Science*, 20(1):13, December 2023. ISSN 1619-697X, 1619-6988. doi: 10.1007/s10287-023-00446-2. URL https://link.springer.com/10.1007/s10287-023-00446-2.

Heasung Kim, Taekyun Lee, Hyeji Kim, and Gustavo de Veciana. Generating Informative Samples for Risk-Averse Fine-Tuning of Downstream Tasks. In *Advances in Neural Information Processing Systems*, 2025.

Daniel Kuhn, Soroosh Shafiee, and Wolfram Wiesemann. Distributionally robust optimization. *Acta Numerica*, 34:579–804, 2025. doi: 10.1017/S0962492924000084.

Mike Laszkiewicz, Johannes Lederer, and Asja Fischer. Marginal tail-adaptive normalizing flows. In *Proceedings of the 39th International Conference on Machine Learning*, 2022.

Jiashuo Liu, Jiayun Wu, Bo Li, and Peng Cui. Distributionally robust optimization with data geometry. In *Advances in Neural Information Processing Systems*, volume 35, 2022.

Casey R. McGrath, Casey D. Burleyson, Zarrar Khan, Aowabin Rahman, Travis Thurber, Chris R. Vernon, Nathalie Voisin, and Jennie S. Rice. tell: a Python package to model future total electricity loads in the United States. *Journal of Open Source Software*, 7(79):4472, 2022. doi: 10.21105/joss.04472.

Paul Michel, Tatsunori Hashimoto, and Graham Neubig. Modeling the second player in distributionally robust optimization. In *International Conference on Learning Representations*, 2021.

Brian Mirletz, Laura Vimmerstedt, Tyler Stehly, Dana Stright, Stuart Cohen, Wesley Cole, Patrick Duffy, David Feldman, Parthiv Kurup, Vignesh Ramasamy, Jarett Zuboy, Gbadebo Oladosu, Jeffrey Hoffmann, Annika Eberle, Owen Roberts, Daniel Mulas Hernando, Greg Avery, Evan Rosenlieb, Anna Schleifer, Dayo Akindipe, Eric Witter, Becca Fuchs, Gabriel Zuckerman, Alex Zolan, Abdalla Abou Jaoude, Levi Larson, Chris Lohse, Nahuel Guaita, Ishita Trivedi, Fred Joseck, Ty Hedalen, Ben Rakov, and Ashok Sekar. 2024 Annual Technology Baseline (ATB) Cost and Performance Data for Electricity Generation Technologies. Technical Report 6006, DOE Open Energy Data Initiative (OEDI); National Renewable Energy Laboratory (NREL), June 2024. URL https://www.osti.gov/biblio/2377191.

Peyman Mohajerin Esfahani and Daniel Kuhn. Data-driven distributionally robust optimization using the Wasserstein metric: performance guarantees and tractable reformulations. *Mathematical Programming*, 171(1-2):115–166, September 2018. ISSN 0025-5610, 1436-4646. doi: 10.1007/s10107-017-1172-1. URL http://link.springer.com/10.1007/s10107-017-1172-1.

Kushagra Pandey, Jaideep Pathak, Yilun Xu, Stephan Mandt, Michael Pritchard, Arash Vahdat, and Morteza Mardani. Heavy-tailed diffusion models. In *International Conference on Learning Representations*, 2025.

Panos Parpas, Berk Ustun, Mort Webster, and Quang Kha Tran. Importance Sampling in Stochastic Programming: A Markov Chain Monte Carlo Approach. *INFORMS Journal on Computing*, 27(2): 358–377, 2015. doi: 10.1287/ijoc.2014.0630.

R. Tyrrell Rockafellar and Stanislav Uryasev. Optimization of conditional value-at-risk. *Journal of Risk*, 2(3):21–41, 2000.

Reuven Y. Rubinstein and Dirk P. Kroese. *The Cross-Entropy Method: A Unified Approach to Combinatorial Optimization, Monte-Carlo Simulation, and Machine Learning*. Springer, New York, 2004.

Herbert Scarf. A min-max solution of an inventory problem. In Kenneth J. Arrow, Samuel Karlin, and Herbert Scarf (eds.), *Studies in the Mathematical Theory of Inventory and Production*, pp. 201–209. Stanford University Press, 1958.

Maurice Sion. On general minimax theorems. *Pacific Journal of Mathematics*, 8(1):171–176, 1958.

Bart P. G. Van Parys, Peyman Mohajerin Esfahani, and Daniel Kuhn. From Data to Decisions: Distributionally Robust Optimization Is Optimal. *Management Science*, 67(6):3387–3402, 2021. doi: 10.1287/mnsc.2020.3678.

Stein W. Wallace and William T. Ziemba (eds.). *Applications of Stochastic Programming*. MPS-SIAM Series on Optimization. SIAM, 2005.

Jie Wang, Rui Gao, and Yao Xie. Sinkhorn distributionally robust optimization. *arXiv preprint arXiv:2109.11926*, 2021.

James Watson and Chris Holmes. Approximate models and robust decisions. *Statistical Science*, 31 (4):465–489, 2016.

Jiaqi Wen and Jianyi Yang. Distributionally Robust Optimization via Generative Ambiguity Modeling, 2026. URL https://arxiv.org/abs/2602.08976. arXiv:2602.08976.

Chen Xu, Jonghyeok Lee, Xiuyuan Cheng, and Yao Xie. Flow-based Distributionally Robust Optimization, February 2024. URL http://arxiv.org/abs/2310.19253. arXiv:2310.19253 [cs].

Ziwei Zhang, Jonathan Yu-Meng Li, and Zhihao Jin. Generative distributionally robust optimization. *arXiv preprint arXiv:2607.24983*, 2026.

Zihao Zhao, Christopher Yeh, Lingkai Kong, and Kai Wang. Diffusion-DFL: Decision-focused Diffusion Models for Stochastic Optimization. In *International Conference on Learning Representations*, October 2026. URL https://openreview.net/forum?id=uhv3f80jmG.

A NEWSVENDOR

A.1 PROBLEM

A retailer chooses order quantities $x \in \mathbb{R}^5_+$ at unit cost, $c(x) = \mathbf{1}^\top x$, before demand $\xi \in \mathbb{R}^5_+$ is observed. Stock of product i ships y_{ij} units to demand for product j along the arcs $\mathcal{E} = \{(j,j)\}_{j=1}^5 \cup \{(j+1,j)\}_{j=1}^4$, and the recourse cost is

$$Q(x,\xi) = \min_{y,u,v\geq 0} \; 0.5\sum_{j=1}^{4} y_{j+1,j} + 100\sum_{j=1}^{5} u_j - 0.25\sum_{i=1}^{5} v_i \tag{11}$$
$$\text{s.t.} \sum_{j:(i,j)\in\mathcal{E}} y_{ij} + v_i = x_i, \qquad \sum_{i:(i,j)\in\mathcal{E}} y_{ij} + u_j = \xi_j, \qquad i,j = 1,\ldots,5,$$

where u_j is unmet demand and v_i leftover stock. The critical ratio is $(100-1)/(100-0.25) = 0.9925$, and recourse is relatively complete, since $y = 0$ is always feasible. The objective is $c(x)$ plus the mean–CVaR equation 3 of $Q(x,\xi)$ with $\beta = 0.25$ and $\alpha = 0.9$.

A.2 Laws and Records

Under the base law $\mathbb{P}_0$, log demand is $0.95\mathcal{N}(\mu, \Sigma) + 0.05\mathcal{N}(\mu + \Delta, \Sigma)$, with $\mu_j = \log 100$, standard deviations 0.35, and correlations 0.6. The shock Δ is 0.9 on products 1, 3, and 5 and 0.225 on products 2 and 4. Each shift family pairs the law the records are drawn from with an out-of-distribution law (Figure 3).

Level. Records from $\mathbb{P}_0$; the shifted law adds 0.35 to every component of μ.

Tail. Records from $\mathbb{P}_0$; the shifted law multiplies the covariance of the shock component by 8, keeping expected demand unchanged.

Support. Records from $\mathbb{P}_0$; the shifted law adds a third component of weight 0.05 whose shock is 1.35 on products 2 and 4 and 0.34 on the others.

Coincidence. Records from a mixture of a calm component of weight 0.75 and five components of weight 0.05, the jth adding Δ_j to product j only; the shifted law is $\mathbb{P}_0$, with the same marginals.

There are 300 records at every N, nested across N, and the level, tail, and support families share them.

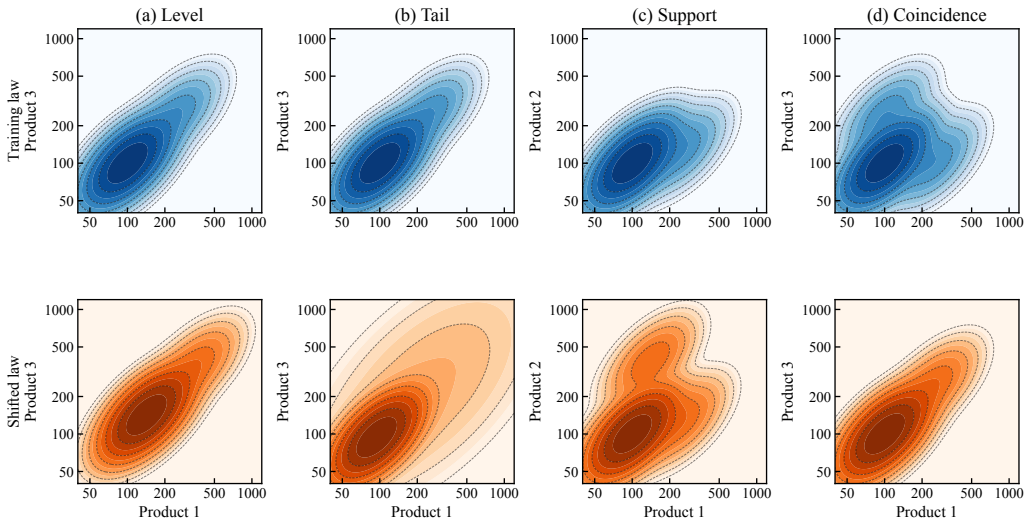


Figure 3: The four newsvendor shift families: joint densities of log demand for products 1 and 3 (1 and 2 in (c)) under the records' law (top) and the shifted law (bottom), with contours spanning 3.5 orders of magnitude so that the shocks are visible. **(a)** Level: the density translates. **(b)** Tail: the shock spreads into a wide, faint band. **(c)** Support: a new component appears where the records' law has almost no mass. **(d)** Coincidence: shocks to one product at a time become joint shocks, with unchanged marginals.

A.3 Learned Nominals

Each nominal, and a heavy-tailed variant of the flow, is fitted to all five products of a record and sampled as a map of $z \sim \mathcal{N}(0, I_5)$, so the weights φ/r_t are exact whether or not the map is invertible (Sec. 4.2). Figure 4 compares them on single records.

Gaussian. Sample mean and covariance of raw demand, with draws clipped at zero.

Copula. The correlation of the normal scores $\Phi^{-1}((m + \frac{1}{2})/N)$ of each coordinate's rank $m \in \{0, \dots, N-1\}$ in the record, with Φ the standard normal distribution function, with draws decoded through the record's empirical quantiles, so they stay within its range.

Log-normal. A maximum-likelihood Gaussian on log demand.

Log-normal mixture. Two components fitted by expectation maximization, the family of the base law, sampled through the inverse of its Rosenblatt transform.

Flow. A RealNVP flow (Dinh et al., 2017) on whitened log demand, with six affine coupling layers of width 16, initialized at the log-normal and fitted by maximum likelihood with Adam. Its number of steps (0 to 400) and weight decay are chosen by five-fold cross-validation, which keeps zero steps on every record at $N = 16$. There the flow remains a log-normal, but with the unbiased covariance (divisor $N - 1$) rather than the maximum-likelihood one (divisor N), so its rows differ from the log-normal's by this 16/15 wider covariance and by independent sampler draws.

Heavy-tailed flow. The tail-adaptive flow of Jaini et al. (2020): the same flow on a Student-t base with a learned number of degrees of freedom per coordinate, obtained by mapping each latent coordinate through Φ and then the Student-t quantile function. Cross-validation chooses among the log-normal, a log-t, and the t-base flow.

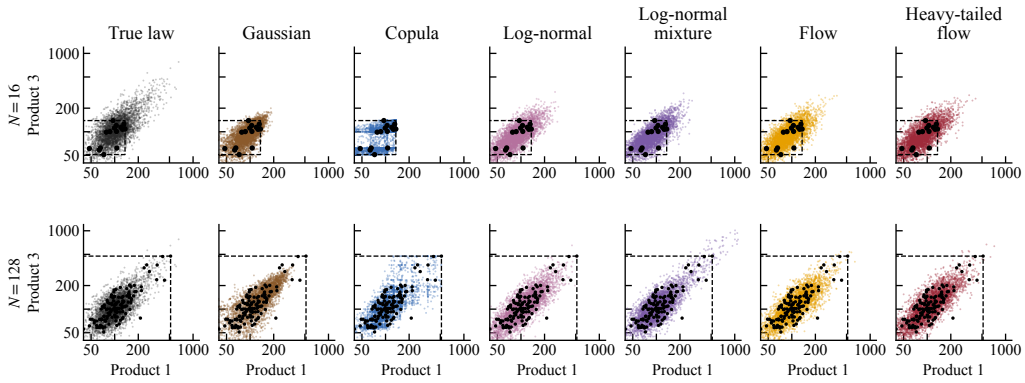


Figure 4: What each nominal can represent: 4,000 draws from each nominal fitted to one record of $N = 16$ (top) and one of $N = 128$ (bottom), shown for products 1 and 3 (black points: the record; dashed box: its range). The copula's draws stay within the record's range, while the other nominals extrapolate beyond it. Here, cross-validation keeps the flow at its log-normal initialization, and the heavy-tailed flow selects a log-t with 30 degrees of freedom.

A.4 Methods

Table 2 summarizes the methods. Methods with a KL ball are run at every radius of the grid $\rho \in \{0, 0.003, 0.005, 0.007, 0.01, 0.015, 0.02, 0.03, 0.05, 0.1, 0.2, 0.4, 0.8\}$, and methods that depend on a decision use the risk-neutral decision $\hat{x}$ on the record and tilt at $\rho_{\mathrm{ref}} = 0.8$.

KL-Rec and SAA. KL-DRO on the empirical distribution (Hu & Hong, 2013). SAA is KL-Rec at $\rho = 0$.

KL-Gen-P and the oracle. One round of the sampler at $\hat{x}$: $M = 256$ latent draws are evaluated, a Gaussian is fitted to their tilt, and $n = 100$ scenarios are drawn from the defensive mixture with $a = 0.9$, once per record for all radii. The oracle applies the same sampler to the true law and serves only as a reference.

KL-Gen. Resamples 100 of 356 draws of the nominal by the tilt, with replacement, matching the $256 + 100$ recourse evaluations of the sampler.

CSSC. Reduces 356 or 1,024 draws of the log-normal or the log-normal mixture to $K = 100$ medoids weighted by cluster mass, clustering each draw's costs under $\hat{x}$ and 32 single-scenario decisions with k-medoids, a scalable variant of the program of Keutchayan et al. (2023).

Transport step. W-DRO and KL-OT move each record point ξ^0 to an approximate maximizer of $Q(x, \xi) - \gamma\|\omega(\xi) - \omega(\xi^0)\|_2^2$, the Lagrangian of a type-2 Wasserstein ball, with ω the standardized log demand, by damped fixed-point steps on the recourse duals. The multiplier γ is set at $\hat{x}$ so that the mean squared displacement is ε times the median squared nearest-neighbor spacing of the record, and we call ε the displacement. Both methods alternate three rounds of moving the points and solving the master.

W-DRO. Moves all N record points, with $\varepsilon \in \{0.01, 0.03, 0.1, 0.3, 1, 3, 10\}$, and has no KL ball.

KL-OT. Moves $\min(100, N)$ record points selected by the tilt, at the displacements of W-DRO, within the ball at every radius of the grid.

Parity. All methods share the records, the evaluation laws, the selection rule, and the master. KL-Gen-P and KL-Gen evaluate the recourse 356 times per record, and KL-Gen's master holds a median of 69 distinct scenarios against the 100 of KL-Gen-P. CSSC evaluates it 33 times per pool draw, and W-DRO and KL-OT about 1,300 times per setting at $N = 16$ and 8,400 to 9,700 at $N = 128$. KL-OT also chooses among 91 settings, against 13 for the other KL methods and 7 for W-DRO. These differences favor the baselines.

Table 2: Newsvendor methods. KL-Gen-P and KL-Gen are run with each nominal of Figure 4, and CSSC with the log-normal and the log-normal mixture. Weights are normalized to sum to one.

Method	Scenarios in the master	Weights	Radius
SAA	the N record points	uniform	0
KL-Rec	the N record points	uniform	grid
KL-Gen-P, oracle	$n = 100$ draws of the sampler	φ/r	grid
KL-Gen	356 draws of the nominal, resampled 100 times by the tilt	$c_i/(356\,\tau_i)$	grid
CSSC	$K = 100$ medoids of 356 or 1,024 draws of the nominal	cluster mass	grid
W-DRO	the N record points, moved	uniform	0
KL-OT	$\min(100, N)$ record points selected by the tilt, moved	uniform	grid

A.5 Solving the Master

The master is a linear program at $\rho = 0$, solved by Gurobi (Gurobi Optimization, LLC, 2026), and otherwise an exponential-cone program solved by Clarabel (Goulart & Chen, 2024). A Clarabel solution is accepted if its value agrees with the objective recomputed at its decision to 10^{-5} relative and is no worse than the solution for $\rho = 0$. Otherwise, a sequential least squares programming solve starts from the solution for $\rho = 0$. This fallback served 10% of the master solves with $\rho > 0$, and 22% of those of KL-Gen-P.

A.6 Selection and Evaluation

Selection rule. Records are split into odd- and even-numbered halves. On each half, each method's setting is chosen as the largest whose mean in-distribution cost is within 5 percentage points of that of SAA, or the cheapest if none is, and it is scored on the other half, so the out-of-distribution law is never consulted. Settings are ordered by radius, by displacement for W-DRO, and by displacement and then radius for KL-OT. Table 1(b) instead reads the frontiers of Figure 5 at a fixed target: the lowest median in-distribution cost among a method's settings whose median out-of-distribution cost is at most half that of SAA, with the stability of the lowest method assessed over 200 bootstrap resamples of the records. Under relative rules that admit in-distribution costs up to 1.10 or 1.25 times that of SAA, the lowest method is unchanged in 7 of the 8 columns of Table 1(a) at 1.10, where the log-normal replaces W-DRO at $N = 128$ under the tail shift, and in all 8 at 1.25.

Scoring. In- and out-of-distribution costs are the objective of App. A.1 under the records' law and the shifted law, as a percentage above the optimum under that law, computed on a scrambled Sobol quadrature with 4,096 points per mixture component. Tables report the median over records with the standard error $1.2533\,\hat{\sigma}/\sqrt{n}$, where $\hat{\sigma}$ is the interquartile range divided by 1.349.

A.7 Full Results

Figure 5 and Tables 3–6 give the full results.

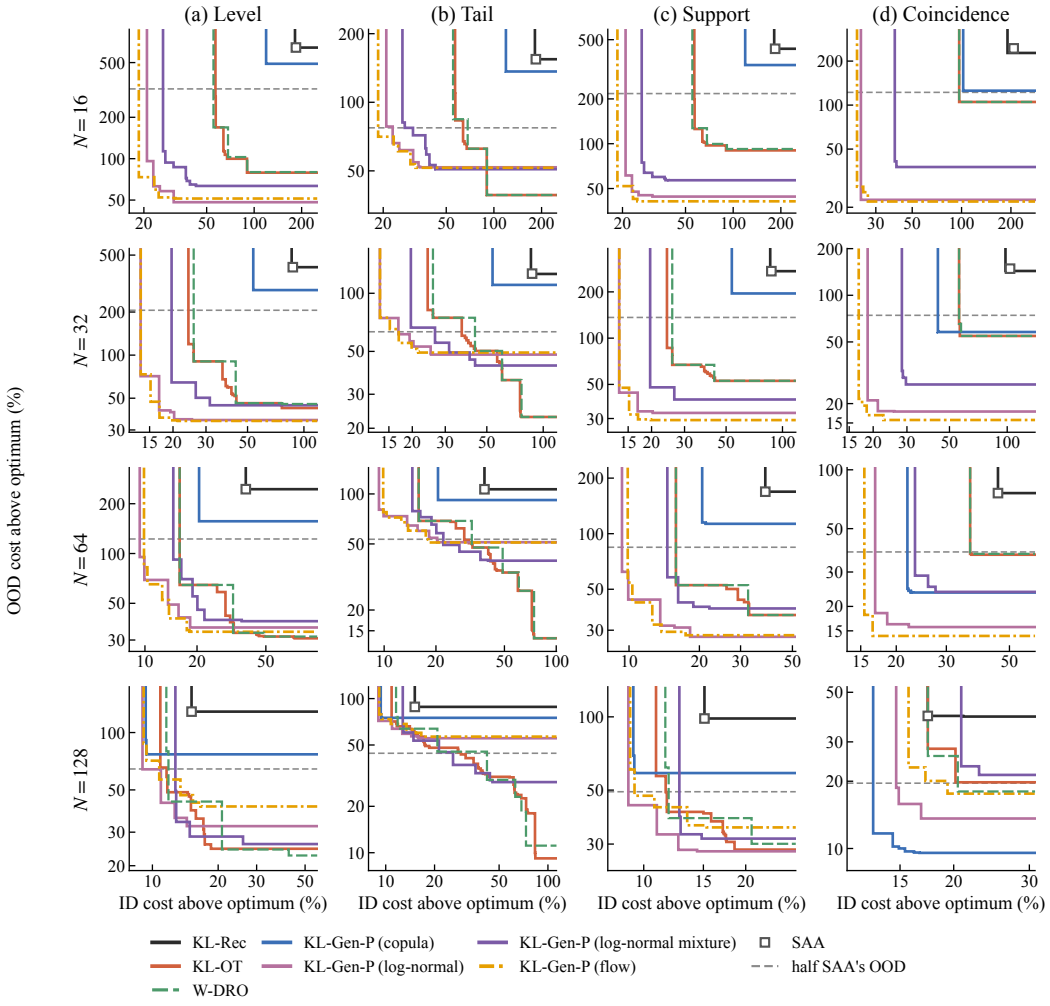


Figure 5: Newsvendor frontiers: out-of-distribution against in-distribution cost above the optimum (%, median over records) as each method's settings vary. Each line is a method's Pareto frontier (lower left is better). Rows are record sizes and columns shifts. The open square is SAA, and the dashed line is half of SAA's out-of-distribution cost, the target of Table 1(b).

Table 3: Newsvendor, every method, $N = 16$ (300 records): cost above the optimum (%) under the level (L), tail (T), support (S), and coincidence (C) shifts. (a) Median out-of-distribution cost ($\pm$ 2 SE) at each method's selection rule. ID cost at $\rho = 0$: median in-distribution cost of the unhedged fit (none for W-DRO and KL-OT). (b) Lowest median in-distribution cost at which a setting halves SAA's median out-of-distribution cost; ·: never. Bold: lowest per column, excluding the oracle; †: lowest in fewer than 80% of bootstrap resamples.

	(a) OOD cost at SAA's ID budget				ID cost	(b) ID cost to halve SAA's OOD			
Method	L	T	S	C	$\rho = 0$	L	T	S	C
SAA	643 ±59	154 ±8	434 ±39	244 ±21	184	·	·	·	·
KL-Rec	647 ±55	155 ±7	435 ±36	227 ±20	184	·	·	·	·
W-DRO	80 ±10	39 ±4	92 ±10	154 ±20	–	55	68	55	97
KL-OT	88 ±11	43 ±4	99 ±11	159 ±20	–	57	64	57	97
Gaussian									
KL-Gen-P	229 ±31	104 ±4	158 ±19	49 ±7	115	40	·	40	42
KL-Gen	480 ±43	135 ±5	316 ±27	128 ±12	116	·	·	·	·
Copula									
KL-Gen-P	490 ±46	136 ±6	338 ±30	126 ±12	125	·	·	·	·
KL-Gen	503 ±48	137 ±6	344 ±30	133 ±13	127	·	·	·	·
Log-normal									
KL-Gen-P	52 ±11	52 ±6	47 ±8	**31** ±5	48	21	23	21	24
KL-Gen	238 ±37	105 ±5	162 ±23	56 ±9	48	43	·	43	40
CSSC	240 ±35	104 ±5	163 ±22	66 ±9	57	44	·	44	45
Log-normal mixture									
KL-Gen-P	65 ±13	52 ±6	59 ±10	44 ±8	41	26	27	26	39
KL-Gen	216 ±34	102 ±5	151 ±20	59 ±8	41	40	·	40	49
CSSC	193 ±35	97 ±6	136 ±24	63 ±9	49	39	·	39	52
Flow									
KL-Gen-P	**52** ±9	52 ±5	**43** ±7	33 ±6	41	**19**	**19**	**19**	**23**†
KL-Gen	229 ±34	103 ±5	152 ±21	49 ±7	38	36	·	36	33
Heavy-tailed flow									
KL-Gen-P	55 ±11	**39** ±4	54 ±11	49 ±8	28	22	22	22	25
KL-Gen	178 ±29	96 ±5	126 ±20	39 ±6	36	31	·	31	31
Oracle (reference)	18 ±3	21 ±2	32 ±3	22 ±3	3				

Table 4: Newsvendor, every method, $N = 32$ (300 records); as Table 3.

	(a) OOD cost at SAA's ID budget				ID cost	(b) ID cost to halve SAA's OOD			
Method	L	T	S	C	$\rho = 0$	L	T	S	C
SAA	412 ±41	126 ±5	273 ±26	149 ±14	87	·	·	·	·
KL-Rec	412 ±41	126 ±5	284 ±27	143 ±13	87	·	·	·	·
W-DRO	46 ±5	**23** ±3	57 ±6	85 ±11	–	26	43	26	56
KL-OT	46 ±5	24 ±3	61 ±6	98 ±12	–	24	37	24	56
Gaussian									
KL-Gen-P	222 ±27	104 ±4	159 ±17	50 ±7	93	·	·	·	37
KL-Gen	414 ±30	127 ±3	278 ±19	119 ±9	90	·	·	·	·
Copula									
KL-Gen-P	285 ±29	111 ±4	195 ±18	58 ±6	61	·	·	·	44
KL-Gen	313 ±29	114 ±4	214 ±19	66 ±8	60	·	·	·	53
Log-normal									
KL-Gen-P	**36** ±7	49 ±5	35 ±5	**23** ±3	37	**13**†	17	**13**†	19
KL-Gen	190 ±24	98 ±4	138 ±16	44 ±7	33	28	·	28	29
CSSC	223 ±26	103 ±4	151 ±18	51 ±7	44	·	·	·	35
Log-normal mixture									
KL-Gen-P	49 ±10	43 ±5	51 ±9	39 ±5	30	20	26	20	28
KL-Gen	168 ±26	94 ±5	124 ±17	48 ±7	32	28	·	28	35
CSSC	160 ±28	90 ±5	119 ±18	54 ±6	32	30	·	30	38
Flow									
KL-Gen-P	41 ±9	55 ±5	**33** ±6	24 ±3	34	13	17	13	**17**
KL-Gen	195 ±28	98 ±4	135 ±18	45 ±7	30	27	·	27	29
Heavy-tailed flow									
KL-Gen-P	44 ±8	37 ±5	46 ±7	43 ±6	24	14	**17**†	14	20
KL-Gen	170 ±24	94 ±4	120 ±16	34 ±5	28	25	·	25	25
Oracle (reference)	19 ±3	21 ±2	32 ±3	23 ±3	3				

Table 5: Newsvendor, every method, $N = 64$ (300 records); as Table 3.

	(a) OOD cost at SAA's ID budget				ID cost	(b) ID cost to halve SAA's OOD			
Method	L	T	S	C	$\rho = 0$	L	T	S	C
SAA	245 ±30	107 ±4	169 ±18	76 ±10	38	·	·	·	·
KL-Rec	264 ±30	108 ±4	182 ±18	78 ±8	38	·	·	·	·
W-DRO	**31** ±4	**34** ±3	44 ±5	37 ±4	–	16	32	16	36
KL-OT	39 ±8	45 ±4	48 ±6	51 ±7	–	16	29	16	36
Gaussian									
KL-Gen-P	245 ±20	107 ±3	172 ±13	55 ±6	90	·	·	·	·
KL-Gen	406 ±21	126 ±2	267 ±13	113 ±8	87	·	·	·	·
Copula									
KL-Gen-P	157 ±18	92 ±3	115 ±11	24 ±4	30	·	·	·	22
KL-Gen	205 ±21	101 ±3	151 ±14	39 ±5	33	·	·	·	26
Log-normal									
KL-Gen-P	39 ±7	52 ±4	31 ±5	**21** ±3	35	**9**†	20	**9**†	17
KL-Gen	204 ±21	101 ±3	145 ±13	43 ±6	34	·	·	·	·
CSSC	209 ±21	101 ±3	151 ±14	45 ±6	42	·	·	·	·
Log-normal mixture									
KL-Gen-P	41 ±9	45 ±5	42 ±6	35 ±5	22	15	22	15	23
KL-Gen	143 ±21	89 ±4	109 ±13	42 ±6	25	·	·	·	·
CSSC	127 ±21	85 ±5	99 ±13	44 ±5	26	24	·	·	·
Flow									
KL-Gen-P	34 ±6	51 ±4	**31** ±4	22 ±3	34	10	**17**	10	**15**
KL-Gen	204 ±22	100 ±3	144 ±14	47 ±6	35	·	·	·	·
Heavy-tailed flow									
KL-Gen-P	35 ±7	43 ±5	35 ±5	28 ±4	25	12	28	12	18
KL-Gen	177 ±20	96 ±3	128 ±13	35 ±5	30	·	·	·	23
Oracle (reference)	19 ±3	22 ±2	30 ±3	25 ±3	3				

Table 6: Newsvendor, every method, $N = 128$ (300 records); as Table 3.

	(a) OOD cost at SAA's ID budget				ID cost	(b) ID cost to halve SAA's OOD			
Method	L	T	S	C	$\rho = 0$	L	T	S	C
SAA	129 ±17	88 ±3	98 ±11	39 ±5	15	·	·	·	·
KL-Rec	141 ±19	89 ±3	111 ±13	39 ±4	15	·	·	·	·
W-DRO	**24** ±5	**45** ±3	**30** ±3	18 ±3	–	12	42	12	20
KL-OT	45 ±8	57 ±4	44 ±6	25 ±3	–	12	29	12	·
Gaussian									
KL-Gen-P	250 ±18	107 ±2	174 ±11	51 ±4	81	·	·	·	·
KL-Gen	389 ±22	124 ±2	261 ±13	103 ±6	82	·	·	·	·
Copula									
KL-Gen-P	77 ±9	75 ±3	60 ±7	**10** ±1	15	·	·	·	**13**
KL-Gen	151 ±16	91 ±3	108 ±11	21 ±3	18	·	·	·	·
Log-normal									
KL-Gen-P	35 ±7	56 ±4	35 ±5	15 ±2	29	**9**†	·	**9**†	15
KL-Gen	189 ±17	99 ±3	134 ±12	40 ±5	34	·	·	·	·
CSSC	202 ±18	101 ±3	140 ±12	41 ±5	40	·	·	·	·
Log-normal mixture									
KL-Gen-P	34 ±8	54 ±5	35 ±5	23 ±4	13	13	**26**	13	·
KL-Gen	106 ±17	82 ±4	85 ±12	39 ±5	19	·	·	·	·
CSSC	96 ±16	79 ±4	81 ±11	36 ±4	17	·	·	·	·
Flow									
KL-Gen-P	41 ±7	58 ±4	35 ±5	18 ±3	33	11	·	9	19
KL-Gen	206 ±20	101 ±3	138 ±13	46 ±5	31	·	·	·	·
Heavy-tailed flow									
KL-Gen-P	56 ±11	68 ±4	45 ±7	49 ±6	24	13	32	13	·
KL-Gen	184 ±19	98 ±3	128 ±12	51 ±6	30	·	·	·	·
Oracle (reference)	9 ±2	37 ±2	18 ±1	14 ±2	3				

B Capacity Expansion

B.1 Model

Variables. Let $\mathcal{Z}$ be the 20 zones, indexed by n, $\mathcal{L}$ the candidate lines with zone-line incidence matrix A, $\mathcal{G}$ the technologies, of which $\mathcal{G}_{\text{th}}$ are gas and $\mathcal{G}_{\text{cont}} = \mathcal{G} \setminus \mathcal{G}_{\text{th}}$ the others, $\mathcal{S}$ the scenarios, and $t = 1, \dots, 24$ the hours of a day. The first stage builds generation capacity x^{gen}_{ng} and transmission capacity x^{tr}_{ℓ} from zero. Gas capacity is $\bar{P}_g u_{ng}$ for a plant count u_{ng}, which is relaxed to be continuous throughout. The recourse variables of scenario s, collected in y_s, are dispatch p_{stng}, flows $f_{st\ell}$, load shedding ℓ^{shed}_{stn}, and battery charge p^{ch}_{stn}, discharge p^{dis}_{stn}, and state of charge e_{stn}.

Objective. Given scenario weights p_s summing to one (App. B.5), the master is

$$\begin{aligned} \min \quad & C^{\text{inv}}(x) + (1-\beta) \sum_{s \in \mathcal{S}} p_s \, \nu \, C^{\text{op}}_s(x, y_s) + \beta \Big(\zeta + \frac{1}{1-\alpha} \sum_{s \in \mathcal{S}} p_s \, v_s \Big) \\ \text{s.t.} \quad & v_s \geq \nu \, C^{\text{op}}_s(x, y_s) - \zeta, \quad v_s \geq 0, \quad \forall s, \qquad C^{\text{inv}}(x) \leq B, \end{aligned} \tag{12}$$

together with the constraints below, where $\nu = 8760/24$ annualizes a day's operating cost, B is the capital budget below, $\beta = 0.25$, $\alpha = 0.9$, and ζ and v_s are the auxiliary variables of the Rockafellar–Uryasev representation of CVaR (Rockafellar & Uryasev, 2000). The investment and operating costs are

$$\begin{aligned} C^{\text{inv}}(x) &= \sum_{n,\, g \in \mathcal{G}_{\text{cont}}} c^{\text{inv}}_g x^{\text{gen}}_{ng} + \sum_{n,\, g \in \mathcal{G}_{\text{th}}} c^{\text{inv}}_g \bar{P}_g u_{ng} + \sum_{\ell \in \mathcal{L}} c^{\text{tr}} |\ell| \, x^{\text{tr}}_{\ell}, \\ C^{\text{op}}_s(x, y_s) &= \sum_{t,n,g} c^{\text{var}}_g p_{stng} + c^{\text{shed}} \sum_{t,n} \ell^{\text{shed}}_{stn}, \end{aligned}$$

where $|\ell|$ is the length of line ℓ, c^{inv}_g and c^{tr} are annualized, and for gas $c^{\text{var}}_g = c^{\text{fuel}} h_g + c^{\text{vom}}_g + c^{\text{CO2}} r^{\text{CO2}} h_g$, with variable operation and maintenance cost c^{vom}_g, heat rate h_g, and emissions rate r^{CO2}.

Constraints. For all s, t, and n, zonal balance is

$$\sum_{g} p_{stng} + p^{\text{dis}}_{stn} - p^{\text{ch}}_{stn} + \ell^{\text{shed}}_{stn} - d_{stn} = (A f_{st})_n,$$

where d_{stn} is the scenario's demand in zone n at hour t, and flows are limited by $-x^{\text{tr}}_{\ell} \leq f_{st\ell} \leq x^{\text{tr}}_{\ell}$, a network-flow model without power-flow constraints. Wind and solar dispatch is bounded by the scenario's capacity factors, $p_{stng} \leq a_{stng} x^{\text{gen}}_{ng}$, and gas dispatch by installed capacity, $p_{stng} \leq \bar{P}_g u_{ng}$. For batteries,

$$0 \leq p^{\text{ch}}_{stn}, p^{\text{dis}}_{stn} \leq x^{\text{gen}}_{n,\text{bat}}, \qquad 0 \leq e_{stn} \leq H x^{\text{gen}}_{n,\text{bat}}, \qquad e_{stn} = e_{s,t-1,n} + \eta^{\text{ch}} p^{\text{ch}}_{stn} - p^{\text{dis}}_{stn} / \eta^{\text{dis}},$$

where $x^{\text{gen}}_{n,\text{bat}}$ is the battery power capacity of zone n, with the last hour linked cyclically to the first. Load shedding satisfies $0 \leq \ell^{\text{shed}}_{stn} \leq \max\{d_{stn}, 0\}$. There are no ramping or unit-commitment constraints.

Capital budget. For each record and seed, B is the investment cost of an unbudgeted plan from a preliminary configuration of KL-Rec at $k = 1$ ($\rho = 0$, $\rho_{\text{ref}} = 0.4$), which ranges from 19.5 to 23.6 bn$/yr, and is shared by every method and radius at $k \leq 1$. At $k = 5$ it is set the same way from runs at $k = 5$.

Network and parameters. The 214 counties of the region of the Electric Reliability Council of Texas (ERCOT) are grouped into 20 zones by k-means on county locations. Dallas and Rockwall counties, which have no coordinates in the source table, take those of the counties with the nearest Federal Information Processing Standards (FIPS) codes. Zonal demand is the sum of county demand, and zonal capacity factors are county averages. Candidate lines join zone centroids along the edges of their Gabriel graph (39 lines, median 177 km). Table 7 gives the cost and technology parameters.

Table 7: Cost and technology parameters, in real 2024 dollars. Generation costs are from the 2024 Annual Technology Baseline of the National Renewable Energy Laboratory (Mirletz et al., 2024) (Moderate scenario, 2030, converted from 2022 dollars by $\times 1.061$), and heat rates are assumed. The gas price and emissions rate are from the Energy Information Administration (Annual Energy Outlook 2024, 2030). Capital costs are annualized with the capital recovery factor $\mathrm{CRF}(r, L) = r(1+r)^L/((1+r)^L - 1)$ over the lifetime L, plus fixed operation and maintenance (O&M). VOM is variable O&M.

Technology	Capital ($/kW)	Fixed O&M ($/kW-yr)	VOM ($/MWh)	Heat rate (MMBtu/MWh)	Lifetime (yr)
Wind	1494	31.0	0.0	–	30
Solar	1266	19.1	0.0	–	30
Gas, combined cycle	1489	33.7	2.2	6.4	30
Gas, combustion turbine	1348	26.5	7.4	9.5	30
Battery 4h	1540	34.5	0.0	–	15

Parameter	Value	Parameter	Value
Lost load c^{shed}	\$10,000/MWh	Discount rate r	7%
Carbon price c^{CO2}	\$150/tCO_2	Gas units (combined cycle, turbine)	500, 150 MW
Gas price c^{fuel}	\$3.43/MMBtu	Battery duration H	4 h
Emissions rate r^{CO2}	0.05306 t/MMBtu	Efficiency $\eta^{\mathrm{ch}} = \eta^{\mathrm{dis}}$	$\sqrt{0.85}$
Transmission c^{tr}	\$1,500/MW-km	Line lifetime, fixed O&M	40 yr, 2%/yr

B.2 Data and Records

Data. The source is hourly county-level ERCOT data: wind and solar capacity factors from Bracken et al. (2023) and demand simulated by the Total ELectricity Load (TELL) model (McGrath et al., 2022), aggregated to the 20 zones. A scenario is one day of 20 zonal demands and 40 zonal capacity factors, so $D = 1{,}440$, cut at local midnight. Short gaps are interpolated, and days with longer gaps are dropped. Table 8 gives the periods.

Table 8: Data periods. Records A to J are the years 2010, 2009, 2007, 2008, 2005, 2001, 2002, 2003, 2004, and 2006. The years 2015–2019 are used only to place 2020 among the other years.

Period	Years	Days	Role
Record	2001–2010	10×364	records and fitted nominals
In distribution (ID)	2011–2014	1,458	evaluation
Out of distribution (OOD)	2020	364	evaluation

Records. At $k = 1$ a record is one year, at $k = \frac{1}{2}$ every second day of it (182 days), and at $k = 5$ one of five sets of five years. Every record is run with five seeds.

Out-of-distribution year. 2020 was designated out of distribution before any method was scored on it, although its days later also served for development (App. B.6). It is the most extreme year of 2001–2020 in the tail of demand: its annual peak (77.4 GW) lies 2.5 standard deviations of year-to-year variation above the 2001–2019 trend. Net load is demand less the output of a fixed reference fleet of 66.0 GW of wind and 25.2 GW of solar, the mean zonal capacities of 25 KL-OT plans at $k = \frac{1}{2}$. The 99th percentile of daily peak net load is 49.6 GW in 2020, against at most 45.7 GW in any other year.

B.3 Learned Nominals

KL-Gen and KL-Gen-P use a conditional normalizing flow, and KL-Gen (copula) and KL-Gen-P (copula) a Gaussian copula with a separate mean and covariance for each season. Both are fitted to the record alone and share their marginal transform and smoothing.

Copula. Each coordinate of a day, in log demand and logit capacity factors, is mapped to its normal score among the record's days, and the scores of each season define a Gaussian. A draw uses one

extra latent coordinate z_0 to choose the season in proportion to the record's season counts, forms the seasonal Gaussian draw from the other coordinates of z, maps each coordinate back through the record's empirical quantiles, and smooths the day over adjacent hours with weights $(0.2, 0.6, 0.2)$.

Flow. The flow replaces the seasonal Gaussian with a model of the 16 leading whitened principal components of the scores, a conditional RealNVP (Dinh et al., 2017) with an affine layer and two coupling layers of width 16 (2,720 parameters), conditioned on two harmonics of the day of the year and on the season. The remaining components follow a seasonal Gaussian. The flow is fitted by maximum likelihood with AdamW, with Gaussian noise of standard deviation 0.3 added to the components, for a number of steps chosen on a season-stratified 20% of the record's days, and then refitted on all of them. All seeds of a record share one flow. In a draw, z_0 selects a record day, whose calendar day and season are the covariates, and the other coordinates drive the flow and the Gaussian remainder. The day is then decoded and smoothed as for the copula.

Properties and fidelity. Before smoothing, each coordinate of a draw of either nominal lies within the record's range, although a draw can combine coordinates into a system-wide peak that no record day reaches. In a separate study on 2001–2010, the flow's held-out log-likelihood exceeded that of a seasonal Gaussian of the copula's form, with tuned shrinkage, in each of the ten years, by a median of 1.06 nats per day with 182 training days and 1.94 with 320. Its configuration was fixed from that study before any plan was scored. The most severe scenarios KL-Gen admits are less spatially coherent in solar than real days (mean correlation of zonal solar profiles 0.84, against 0.88 for the 20 most severe days of 2020). The copula overstates the frequency of the decade's tail: the share of its draws whose peak net load exceeds the 2001–2010 99th percentile is about 1.8 times the decade's own share. This statistic was not computed for the flow.

B.4 METHODS

Table 9 summarizes the methods. KL-Rec, KL-Gen, KL-Gen-P, their copula variants, and KL-OT share the adaptive loop of Algorithm 1:

Rounds. The initial plan solves the unbudgeted, risk-neutral problem on one scenario fixed by the seed. Each of twelve rounds evaluates $M = 256$ candidates at the current plan (192 for the proposal methods, which spend 64 more evaluations fitting the proposal), tilts them at ρ_{ref}, and admits $n = 4$, so the master holds at most 48 scenarios.

Base weights. A new scenario's base weight, $c_i/(M\tau_i)$, or $c_i b_i/\tau_i$ for the proposal methods, where $b_i \propto \varphi(z_i)/r_t(z_i)$ and $\tau_i \propto b_i \exp(Q_i/\lambda_t)$, is fixed at admission, and the weights of all rounds are normalized together.

Master. Each round recomputes the worst case at the current plan (App. B.5) and solves for the next plan. The last plan is reported.

Radii. KL-Rec, KL-OT, and the copula variants are run at $k \le 1$ at the eleven pairs with $\rho_{\mathrm{ref}} \in \{0.2, 0.4\}$, $\rho \in \{0, 0.02, 0.05, 0.1, 0.2, 0.4\}$, and $\rho \le \rho_{\mathrm{ref}}$. KL-Gen, KL-Gen-P, and every method at $k = 5$ are run at the five pairs $(0.2, 0)$, $(0.2, 0.05)$, $(0.2, 0.2)$, $(0.4, 0)$, and $(0.4, 0.05)$.

The methods differ as follows.

KL-Rec. Candidates are record days drawn with replacement.

KL-Gen. Candidates are draws of the flow.

KL-Gen-P. Candidates are 192 draws from a proposal that shifts the mean of φ (the mean-shift case of Sec. 4.3) in a 10-dimensional active subspace (Constantine, 2015) of the cost gradients of 64 fitting draws, mixed with φ at $a = 0.5$. Four are resampled by the tilt.

KL-Gen (copula) and KL-Gen-P (copula). KL-Gen and KL-Gen-P with the copula in place of the flow, with all else identical. The tables report KL-Gen (copula).

KL-OT (δ). Candidates are 256 record days. From the second round, each is moved before evaluation to an approximate maximizer of $Q(x_t, \xi) - \gamma\|\omega(\xi) - \omega(\xi^0)\|_2^2$, the Lagrangian of a type-2 Wasserstein ball, where ξ^0 is the record day and ω its standardized log demand and logit capacity factors, by three damped fixed-point steps on the dispatch subgradient. A moved day keeps its record day's base weight. The multiplier γ is set once, at the second round, so that the mean cost

increase of moved days is δ times the mean cost of the unmoved candidates. The transport budget $\delta \in \{0.3, 1, 3\}$ is thus a cost-increase target at one plan rather than a radius.

W-DRO (δ). Holds 48 record days with uniform weights and no KL ball. Each round moves every day by the step of KL-OT, with γ set as for KL-OT, to the target δ, at the first plan, and re-solves the master on each day's largest penalized cost, for at most four rounds. At $\delta = 1$ most runs reach the four-round cap, with a median relative gap of about 5×10^{-3}.

CSSC. Selects 48 days from 256 record days (all 182 at $k = \frac{1}{2}$) by the clustering program of Keutchayan et al. (2023), with opportunity costs $C^{\mathrm{inv}}(x_i^*) + \nu\, Q(x_i^*, \xi_j)$ for the plan x_i^* that solves the problem on day i alone, and weights them by cluster mass. It has no KL ball.

SAA. Solves the master on 48 record days with uniform weights.

Table 9: Capacity expansion methods. All use the objective in equation 12 with $\beta = 0.25$, $\alpha = 0.9$, and the budget B of the record and seed.

Method	Candidates per round	Scenarios in the master	Weights
KL-Rec	256 record days	at most 48, four per round	KL worst case at ρ
KL-Gen	256 draws of the flow	same	same
KL-Gen-P	192 draws from a fitted proposal	same	same
KL-Gen (copula)	256 copula draws	same	same
KL-Gen-P (copula)	192 draws from a proposal fitted to the copula	same	same
KL-OT (δ)	256 record days, moved from the second round	same	same
W-DRO (δ)	a moved copy of each day, from the second round	48 record days, each valued at its largest penalized cost over the day and its moved copies	$1/48$
CSSC	256 record days (all 182 at $k = \frac{1}{2}$)	48 selected	cluster masses
SAA	none	48 record days	$1/48$

B.5 Solving the Master

The worst case. For the mean–CVaR risk measure, with $Q_i := Q(x, \xi_i)$ and normalized base weights $\bar{w}$, the adversary maximizes $\min_\zeta\{\zeta + \sum_i p_i\, \psi_\zeta(Q_i)\}$ over the ball $\mathcal{B}_\rho$ of probability vectors p with $\sum_i p_i \log(p_i/\bar{w}_i) \le \rho$. The objective is linear in p and convex in ζ and the feasible set is convex and compact, so the maximum and minimum may be exchanged (Sion, 1958). For fixed ζ the maximizer is the tilt $p_i \propto \bar{w}_i \exp(\psi_\zeta(Q_i)/\lambda)$, with λ bisected so that the KL constraint binds, and ζ is found by golden-section search over $[\min_i Q_i, \max_i Q_i]$.

The alternation. Each round solves the linear program equation 12 at the worst-case weights computed at the current plan, so the reported plan x_T is a best response to the worst case at x_{T-1}. Weak duality bounds its optimality gap. With $J(x, p)$ the objective of equation 12, $\overline{V}(x) = \max_{p \in \mathcal{B}_\rho} J(x, p)$, and $\underline{V}(p) = \min_x J(x, p)$, the gap is at most $\overline{V}(x_T) - \max\{\underline{V}(p_T), \underline{V}(p')\}$, where p_T are the final weights and p' is the worst case at x_T; evaluating $\underline{V}(p')$ costs one more master solve. On the final scenario sets of 150 runs of KL-Rec, KL-OT, and a copula variant without hourly smoothing at $(\rho_{\mathrm{ref}}, \rho) = (0.2, 0.05)$ and $k = \frac{1}{2}$, the median bound is 0.02 to 0.15 bn\$/yr by method, under 0.5% of the objective, and one further step changes the median ID and OOD costs by at most 0.15 bn\$/yr.

Solver and computation. Masters are built in CVXPY (Diamond & Boyd, 2016) and solved by the Gurobi barrier method (Gurobi Optimization, LLC, 2026) on 8 threads, and the candidates' recourse costs are evaluated in parallel on 8 cores. Excluding the ID and OOD scoring and the fitting of the nominal, a run at $k = \frac{1}{2}$ and $(\rho_{\mathrm{ref}}, \rho) = (0.2, 0.05)$ takes a median of 7 to 8 minutes for KL-Rec and the generative methods, 16 minutes for KL-OT, and 19 minutes for W-DRO. CSSC runs, including the clustering, take at most 43 minutes.

B.6 Evaluation and Statistics

Scoring. The final plan of every run is scored by the objective in equation 12 with uniform weights over all ID or OOD days.

Statistics. Paired differences between methods at the same seed are summarized by their median over the five seeds, so the record is the unit of analysis: ten records at $k = \frac{1}{2}$, five (A to E) at $k = 1$, and five five-year blocks at $k = 5$. Table 11 gives the median over records with its standard error, the standard deviation over records divided by the square root of their number, and a two-sided Wilcoxon signed-rank test.

Development. The radii, the risk weight β, the marginals and smoothing of the nominals, and the construction of the base weights were chosen after comparing configurations on the ID and OOD days, which therefore served for development as well as for evaluation. The flow's architecture and training were fixed before any plan was scored (App. B.3), and it shares the copula's marginals and smoothing.

Severity. A day's severity is its system peak net load, with net load as in App. B.2, and its peak hour is the hour of that peak. The OOD days of Figure 2 are the 20 most severe days of 2020 (41.8 to 53.7 GW), and a method's most severe scenarios are the top 10% by severity of the scenarios it admits, 48 per run, pooled over record years and seeds at $(\rho_{\mathrm{ref}}, \rho) = (0.2, 0.05)$.

Figure 2(a). Each point is a setting's median over records of the median over seeds, and a method's frontier joins its non-dominated settings. KL-OT at $\delta = 3$ was run at three of the five radius pairs, and W-DRO is a single point. Further radius pairs of KL-Rec and KL-OT are dominated by the KL-Gen points shown.

Figure 2(b). The maps show zonal wind capacity factors, standardized per zone over the day and clipped at ± 2, on the most severe day of 2020 and on each method's most severe admitted scenario over all 50 runs. Spatial coherence is the mean correlation of the 24-hour profiles over the 190 pairs of zones, over daylight hours for solar. Boxes span the interquartile range, whiskers the 10th to 90th percentiles, and the gray band is the interquartile range over the 20 OOD days.

Figure 2(c). Each day is represented by its 20 zonal net loads at its peak hour, standardized per zone over 2001–2010. The horizontal axis is peak net load relative to the median OOD day. The vertical axis is the distance to the nearest real day of 2001–2010 outside the record's year, after the scenario's demand is scaled so that its system net load equals that day's, so only the spatial shape counts. Small markers are medians per record, large markers medians over records, the star the median OOD day, and the dotted lines the OOD days' median severity and the median distance of the decade's own most severe days. A small distance marks a shape common among real days but does not prove realism. Over the full day (24 hours of demand, wind, and solar), the most severe scenarios of KL-Gen lie 0.417 from the nearest real day of 2011–2014 and 2020, against 0.367 for real days of the same severity and 0.372 for KL-OT ($\delta = 1$). Compared with each OOD day, the nearest admitted scenarios of KL-Gen lie within 0.15 of the OOD days' demand level, against 0.4 to 0.8 below for KL-OT and KL-Rec, while, with demand rescaled, the three methods' shape distances are nearly the same.

Figure 2(d). Demand is system demand at the scenario's peak hour, relative to the largest such value over the 2001–2010 days (72.6 GW), and wind is system wind output at that hour under the reference fleet. Gray points are the 2001–2010 days; some of them, and one scenario of KL-OT ($\delta = 3$), lie outside the axes.

Reported settings. KL-OT and W-DRO were also run at $\delta \in \{0.3, 3\}$, KL-OT at four radius pairs for $k \leq 1$ and two for $k = 5$. These settings never reach the Pareto front, so the tables report $\delta = 1$, and Figure 2 also shows KL-OT at $\delta = 3$.

B.7 Full Results

Tables 10 and 11 give the full results; the copula ablation is the two KL-Gen (copula) columns of Table 10 and the two KL-Gen − KL-Gen (copula) columns of Table 11. Figure 6 shows that the two radii act as designed, and Figure 7 summarizes KL-Gen's advantage across record lengths.

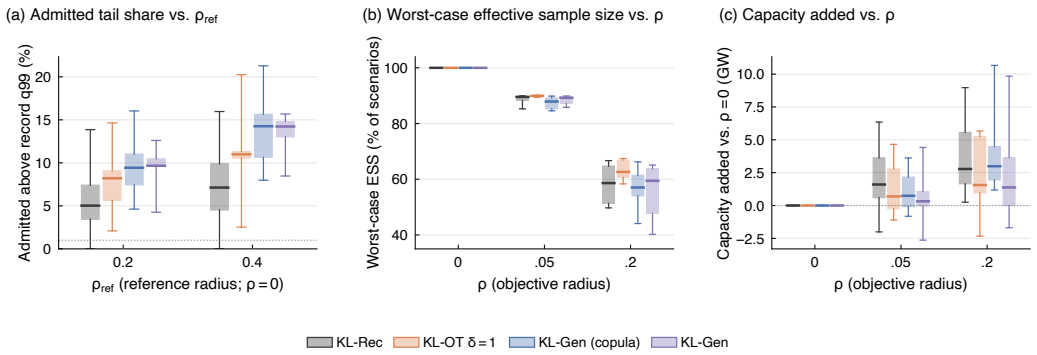


Figure 6: The two radii act as designed (capacity expansion, $k = \frac{1}{2}$). Boxes span the interquartile range over the ten records (each the median over five seeds; in (a), seeds are pooled), and whiskers the full range. **(a)** Share of admitted scenarios above the record's 99th percentile of peak net load, at $\rho = 0$ (dotted: the record's own 1 %). Raising ρ_{ref} admits more severe scenarios, in 39 of 40 (method, record) pairs. **(b)** Effective sample size of the worst-case weights, as a share of the admitted scenarios, at $\rho_{\text{ref}} = 0.2$. It falls as ρ grows, and the realized divergence equals ρ in every run. **(c)** Capacity added relative to $\rho = 0$ (GW) at $\rho_{\text{ref}} = 0.2$, paired within record and seed. Capital is fixed by the budget, so ρ changes the mix rather than the spend.

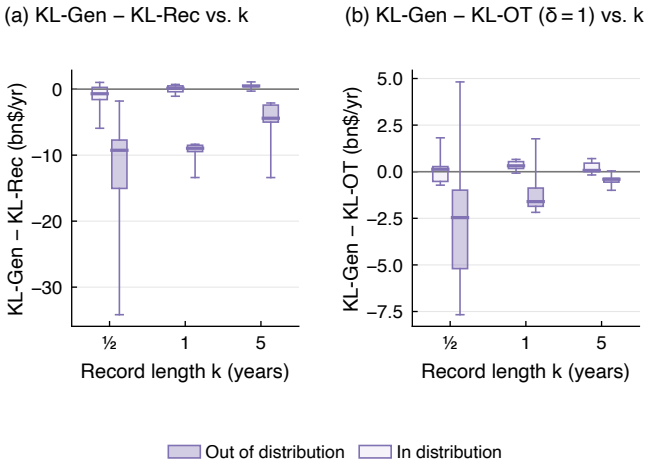


Figure 7: KL-Gen's advantage across record lengths (capacity expansion). Paired cost difference (bn$/yr; negative: KL-Gen is cheaper) against **(a)** KL-Rec and **(b)** KL-OT ($\delta = 1$), out of distribution (filled) and in distribution (light). Each record contributes the median over the five radius pairs of Table 10 of its median over seeds. Boxes span the interquartile range over records and whiskers the full range. The out-of-distribution gap shrinks as the record grows, and the in-distribution differences stay within about 1 bn$/yr of zero.

Paired comparisons. Table 11 compares methods at the same radius pair $(\rho_{\text{ref}}, \rho)$. With five records at $k = 1$ and five blocks at $k = 5$, no difference can reach $p < 0.05$, so we report the number of records in which the first method is cheaper.

KL-Gen vs. KL-Rec. KL-Gen's out-of-distribution cost is lower at every radius pair:

- at $k = \frac{1}{2}$, by 10.0–15.6 bn$/yr, in 10 of 10 records ($p < 0.01$ at all five pairs);
- at $k = 1$, by 8.3–10.7 bn$/yr, in 5 of 5 records;
- at $k = 5$, by 3.0–5.7 bn$/yr, in 4–5 of 5 blocks.

Table 10: Capacity expansion: in-distribution (2011–2014) and out-of-distribution (2020) cost (bn$/yr) at the five radius pairs $(\rho_{\mathrm{ref}}, \rho)$ run at every k, and of SAA, CSSC, and W-DRO, which have no KL radii (median over records of the median over five seeds). Standard errors over records are 0.02–0.9 in distribution and 0.05–3.9 out of distribution for the methods with radii, and up to 3.3 and 9.2 for the others. Table 11 gives paired differences. Bold: on the Pareto front at that k. KL-OT and W-DRO use $\delta = 1$. Further radius pairs run at $k \leq 1$ are dominated by settings shown.

		In-distribution					Out-of-distribution				
ρ_{ref}	ρ	KL-Rec	KL-OT	KL-Gen	KL-Gen-P	KL-Gen (copula)	KL-Rec	KL-OT	KL-Gen	KL-Gen-P	KL-Gen (copula)
$k = \frac{1}{2}$ (10 record years)											
0.2	0	32.08	30.07	29.97	29.99	29.97	50.75	37.44	33.74	33.49	35.43
	0.05	31.63	29.99	30.43	30.56	30.33	48.25	35.67	33.25	32.73	33.16
	0.2	30.84	30.31	30.65	30.79	30.77	45.27	36.54	33.61	32.84	34.86
0.4	0	31.85	30.08	**29.83**	30.08	**29.83**	49.38	39.77	**33.18**	33.57	**33.57**
	0.05	30.44	30.10	30.43	**30.38**	**30.17**	43.13	35.98	32.64	**32.60**	**32.69**
SAA				38.56					73.33		
CSSC				33.95					45.78		
W-DRO				30.46					35.32		
$k = 1$ (5 record years)											
0.2	0	30.26	**29.66**	29.82	**29.82**	29.88	43.84	**34.59**	32.51	**32.49**	33.28
	0.05	30.11	29.87	30.72	30.60	30.30	44.13	34.10	32.36	32.67	32.67
	0.2	30.52	30.27	30.65	30.94	30.69	41.34	35.06	32.55	32.76	32.80
0.4	0	29.77	29.70	**29.99**	30.00	**29.71**	42.40	35.97	**32.20**	32.41	**32.72**
	0.05	29.87	**29.61**	30.69	30.50	**30.17**	40.42	**35.32**	32.35	32.27	**32.09**
SAA				36.66					65.74		
CSSC				33.60					44.93		
W-DRO				30.46					33.83		
$k = 5$ (5 record blocks)											
0.2	0	29.42	29.70	29.88	29.61	**29.56**	39.65	34.38	32.45	32.68	**32.60**
	0.05	29.40	29.77	30.29	30.30	30.03	37.46	32.90	32.40	32.18	32.93
	0.2	29.77	30.18	30.69	30.45	30.22	38.34	33.06	32.91	32.56	33.07
0.4	0	**29.36**	**29.51**	29.83	**29.68**	29.68	**36.61**	**32.65**	32.95	**32.40**	32.86
	0.05	**29.38**	29.89	**30.46**	**30.32**	**30.18**	**35.29**	32.79	**32.04**	**32.06**	**32.10**
SAA				38.80					75.86		
CSSC				33.47					40.51		
W-DRO				33.16					38.05		

The gap shrinks as the record grows. In distribution, KL-Gen is cheaper at $k = \frac{1}{2}$ (by 0.05–1.35 bn$/yr), mixed at $k = 1$, and 0.3–0.9 bn$/yr more expensive at $k = 5$.

KL-Gen vs. KL-OT. KL-Gen's out-of-distribution cost is lower at 14 of the 15 radius pairs:

- at $k = \frac{1}{2}$, by 1.7–3.1 bn$/yr, in 6–10 of 10 records ($p < 0.05$ at two pairs);
- at $k = 1$, by 1.3–2.0 bn$/yr, in 4–5 of 5 records;
- at $k = 5$, by 0.4–1.1 bn$/yr at four pairs, and 0.4 bn$/yr higher at $(0.4, 0)$.

In distribution the two are indistinguishable at $k = \frac{1}{2}$. At $k \geq 1$, KL-Gen costs 0.07–0.99 bn$/yr more, and is cheaper in at most 2 of 5 records. At the same radii, KL-Gen therefore trades a small in-distribution premium for lower out-of-distribution cost.

Ablations. The proposal variant stays within 0.8 bn$/yr of KL-Gen on both axes; one of its 30 differences is significant (-0.80 out of distribution at $k = \frac{1}{2}$, $(0.2, 0.2)$). Out of distribution, KL-Gen and KL-Gen (copula) are within two standard errors of each other at every radius pair and k. In distribution, the copula is 0.15–0.45 bn$/yr cheaper at $k \geq 1$, beyond two standard errors at two of five pairs for each k. Replacing the copula with the flow thus leaves out-of-distribution cost unchanged and adds a small in-distribution premium when the record is longer.

Table 11: Capacity expansion: paired cost differences (bn$/yr; negative: the first method is cheaper) at each radius pair of Table 10: the median over records (standard error) of each record's median over seeds. */**: two-sided Wilcoxon signed-rank $p < 0.05/0.01$ over records. With five records ($k = 1$) or blocks ($k = 5$), the smallest attainable p is 0.0625.

		In-distribution				Out-of-distribution			
ρ_{ref}	ρ	KL-Gen − KL-Rec	KL-Gen − KL-OT	KL-Gen-P − KL-Gen	KL-Gen − KL-Gen (copula)	KL-Gen − KL-Rec	KL-Gen − KL-OT	KL-Gen-P − KL-Gen	KL-Gen − KL-Gen (copula)
$k = \frac{1}{2}$ *(10 record years)*									
0.2	0	-1.35 (0.63)*	-0.11 (0.30)	-0.02 (0.21)	-0.07 (0.18)	-15.62 (2.80)**	-1.79 (1.41)*	-0.80 (0.60)	-0.30 (1.03)
	0.05	-0.89 (0.70)	$+0.15$ (0.18)	$+0.03$ (0.15)	$+0.05$ (0.14)	-10.89 (3.13)**	-2.12 (1.45)	-0.17 (0.77)	-0.12 (0.64)
	0.2	-0.48 (0.77)	$+0.47$ (0.52)	-0.07 (0.32)	$+0.08$ (0.23)	-10.63 (2.95)**	-1.65 (1.28)	-0.80 (0.93)*	-0.46 (1.39)
0.4	0	-1.29 (0.64)*	-0.31 (0.26)	-0.02 (0.14)	$+0.14$ (0.18)	-13.27 (2.45)**	-3.10 (1.88)	-0.10 (0.30)	-0.28 (0.63)
	0.05	-0.05 (0.81)	$+0.21$ (0.22)	$+0.10$ (0.10)	-0.06 (0.11)	-9.99 (3.23)**	-3.12 (0.80)**	-0.13 (0.65)	$+0.21$ (0.34)
$k = 1$ *(5 record years)*									
0.2	0	-0.15 (0.43)	$+0.36$ (0.39)	-0.07 (0.39)	$+0.26$ (0.35)	-9.50 (1.85)	-1.29 (2.24)	-0.03 (1.89)	-0.05 (0.43)
	0.05	$+0.53$ (0.28)	$+0.72$ (0.13)	$+0.24$ (0.20)	$+0.41$ (0.05)	-10.70 (0.97)	-1.60 (0.82)	-0.12 (0.23)	-0.07 (0.41)
	0.2	$+0.10$ (0.82)	$+0.10$ (0.25)	$+0.17$ (0.11)	$+0.28$ (0.44)	-8.35 (0.55)	-1.57 (1.02)	-0.03 (0.33)	-0.56 (1.48)
0.4	0	-0.10 (0.49)	$+0.17$ (0.10)	-0.05 (0.08)	$+0.19$ (0.13)	-9.59 (1.00)	-2.02 (0.45)	-0.31 (0.59)	-0.35 (0.62)
	0.05	$+0.76$ (0.39)	$+0.99$ (0.28)	-0.01 (0.14)	$+0.45$ (0.16)	-8.26 (1.24)	-1.75 (0.54)	-0.11 (0.32)	$+0.12$ (0.09)
$k = 5$ *(5 record blocks)*									
0.2	0	$+0.36$ (0.25)	$+0.12$ (0.17)	-0.18 (0.09)	$+0.18$ (0.10)	-5.70 (1.76)	-1.10 (0.41)	$+0.21$ (0.14)	-0.24 (1.05)
	0.05	$+0.71$ (0.41)	$+0.33$ (0.20)	$+0.06$ (0.13)	$+0.25$ (0.19)	-5.00 (3.08)	-0.44 (0.34)	-0.04 (0.04)	$+0.04$ (0.24)
	0.2	$+0.33$ (0.27)	$+0.46$ (0.18)	-0.38 (0.18)	$+0.39$ (0.07)	-4.37 (2.01)	-0.49 (0.22)	-0.19 (0.21)	-0.24 (0.31)
0.4	0	$+0.33$ (0.21)	$+0.30$ (0.13)	-0.07 (0.09)	$+0.27$ (0.08)	-3.14 (1.75)	$+0.39$ (1.06)	-0.75 (0.51)	$+0.82$ (0.68)
	0.05	$+0.90$ (0.13)	$+0.07$ (0.17)	$+0.02$ (0.07)	$+0.15$ (0.09)	-2.98 (0.57)	-0.35 (0.15)	-0.04 (0.13)	-0.23 (0.29)